Paleoceanography and Paleoclimatology

RESEARCH ARTICLE
10.1029/2019PA003708

Special Section:
Special Collection to Honor the Career of Robert C. Thunell

Key Points:
- The Arctic Ocean experienced warm sea-surface temperatures and seasonally sea ice-free conditions during interglacial Marine Isotope Stage 11
- Peak warmth and minimal sea ice occurred during the middle to late part of the interglacial followed by increased land ice and ice shelves
- Heinrich-like events occurred in the Arctic during the MIS 12-MIS 11 transition (Termination V) and during the MIS 11-MIS 10 transition

Supporting Information:
- Supporting Information S1
- Data Set S1

Correspondence to:
T. M. Cronin,
tcronin@usgs.gov

Citation:
Cronin, T. M., Keller, K. J., Farmer, J. R., Schaller, M. F., O'Regan, M., Poirier, R., et al. (2019). Interglacial paleoclimate in the Arctic. *Paleoceanography and Paleoclimatology*, *34*, 1959–1979. https://doi.org/10.1029/2019PA003708

Received 1 JUL 2019
Accepted 16 OCT 2019
Accepted article online 13 NOV 2019
Published online 7 DEC 2019

Interglacial Paleoclimate in the Arctic

Thomas M. Cronin[1], Katherine J. Keller[1,2], Jesse R. Farmer[3,4], Morgan F. Schaller[5], Matt O'Regan[6], Robert Poirier[7], Helen Coxall[6], Gary S. Dwyer[8], Henning Bauch[9], Ingalise G. Kindstedt[1,10], Martin Jakobsson[6], Rachel Marzen[7], and Emiliano Santin[11]

[1]Florence Bascom Geoscience Center, U.S. Geological Survey, Reston, VA, USA, [2]Department of Earth and Planetary Sciences, Harvard University, Cambridge, MA, USA, [3]Department of Geosciences, Princeton University, Princeton, NJ, USA, [4]Department of Climate Geochemistry, Max-Planck Institute for Chemistry, Mainz, Germany, [5]Earth and Environmental Science, Rensselaer Polytechnic Institute, Troy, NY, USA, [6]Department of Geological Sciences, Stockholm University, Stockholm, Sweden, [7]Lamont-Doherty Earth Observatory, Columbia University, Palisades, NY, USA, [8]Nicholas School of the Environment, Duke University, Durham, NC, USA, [9]GEOMAR Helmholtz-Zentrum für Ozeanforschung Kiel, Kiel, Germany, [10]University of Maine Climate Change Institute, University of Maine, Orono, ME, USA, [11]Atmospheric, Oceanic, and Earth Sciences, George Mason University, Fairfax, VA, USA

Abstract Marine Isotope Stage 11 from ~424 to 374 ka experienced peak interglacial warmth and highest global sea level ~410–400 ka. MIS 11 has received extensive study on the causes of its long duration and warmer than Holocene climate, which is anomalous in the last half million years. However, a major geographic gap in MIS 11 proxy records exists in the Arctic Ocean where fragmentary evidence exists for a seasonally sea ice-free summers and high sea-surface temperatures (SST; ~8–10 °C near the Mendeleev Ridge). We investigated MIS 11 in the western and central Arctic Ocean using 12 piston cores and several shorter cores using proxies for surface productivity (microfossil density), bottom water temperature (magnesium/calcium ratios), the proportion of Arctic Ocean Deep Water versus Arctic Intermediate Water (key ostracode species), sea ice (epipelagic sea ice dwelling ostracode abundance), and SST (planktic foraminifers). We produced a new benthic foraminiferal $\delta^{18}O$ curve, which signifies changes in global ice volume, Arctic Ocean bottom temperature, and perhaps local oceanographic changes. Results indicate that peak warmth occurred in the Amerasian Basin during the middle of MIS 11 roughly from 410 to 400 ka. SST were as high as 8–10 °C for peak interglacial warmth, and sea ice was absent in summers. Evidence also exists for abrupt suborbital events punctuating the MIS 12-MIS 11-MIS 10 interval. These fluctuations in productivity, bottom water temperature, and deep and intermediate water masses (Arctic Ocean Deep Water and Arctic Intermediate Water) may represent Heinrich-like events possibly involving extensive ice shelves extending off Laurentide and Fennoscandian Ice Sheets bordering the Arctic.

1. Introduction

The climatic interval known as the Marine Isotope Stage 11 (MIS 11) was a long (~40,000–50,000 years), warm interglacial period with the warmest temperatures and highest global sea level between ~410 and 400 ka (kiloannum). MIS 11 climate has puzzled researchers for years because orbital insolation patterns and atmospheric CO_2 concentrations were like those of the Holocene interglacial (Masson-Delmotte et al., 2006), but many paleo-records and climate models indicate higher global sea level and warmer climatic conditions (Past Interglacials Working Group of PAGES, 2016), especially at higher latitudes (de Vernal & Hillaire-Marcel, 2008).

MIS 11 sea level was probably 6 to 13 meters above present sea level (Dutton et al., 2015); however, higher (up to 20 m; Olson & Hearty, 2009) and lower (near present sea level; Bowen, 2010, Bauch & Erlenkeuser, 2003) global estimates and regional variability exist (Raymo & Mitrovica, 2012; see Rohling et al., 2009; Elderfield et al., 2012; Spratt & Lisiecki, 2016). Nonetheless, on a global scale, sea level during MIS 11 is generally believed to have been higher than in both Holocene and last interglacial periods (MIS 5e, Eemian, ~6–9 m above present, Kopp et al., 2009). While SST were higher than Holocene in the Atlantic Ocean (Bauch et al., 2000) and lower in other regions (Milker et al., 2013), there is evidence they were relatively stable compared to the Holocene (Kandiano et al., 2017; Palumbo et al., 2019).

In addition to high global sea level and warm climatic conditions, the duration of MIS 11, by some estimates up to 40 kyr long (Berger & Loutre, 2002; McManus et al., 1999; Rohling et al., 2010), exceeds that of other

Quaternary interglacials. For example, at Ocean Drilling Program (ODP) Site 646 south of Greenland, the dominant spruce (*Picea*) and fir (*Abies*) pollen signify an extended (nearly 50 kyr) MIS 11 interglacial with a "nearly ice-free Greenland" and higher than present North Atlantic SST in the western subpolar North Atlantic (de Vernal & Hillaire-Marcel, 2008). The latter, however, contrasts with the Nordic seas, where rather cold SST persisted during MIS 11 probably caused by a massive impact of MIS 12 deglaciation on surface stratification and winter sea ice formation (Kandiano et al., 2012, 2016; Thibodeau et al., 2018). Moreover, the presence of ice-rafted debris (IRD) across MIS 11 in the southwestern Nordic seas would argue for continual iceberg presence there and for an existing east Greenland Ice Sheet with glaciers reaching down to sea level.

Understanding high-latitude cryospheric and climate variability during MIS 11 helps determine the sensitivity of Greenland and Antarctic Ice Sheets to atmospheric CO_2 (Jouzel et al., 2007); the role of orbitally driven insolation (Rohling et al., 2010; Willeit et al., 2019; Yin & Berger, 2015); the phenomenon of Arctic Amplification, that is, amplified warming in Arctic regions due to sea ice loss and other processes, relative to global mean temperature (Cronin et al., 2017); and the potential for abrupt, millennial scale events during warm climate intervals (McManus et al., 1999). Importantly, MIS 11 is also relevant for understanding the evolution of climate during the Holocene interglacial, specifically for distinguishing natural climate variability from anthropogenic influence on climate (Palumbo et al., 2019; Ruddiman, 2007).

The current study examines the paleoceanography of the Arctic Ocean during MIS 11 using several proxies from sediment cores located mainly in the western and central Arctic Ocean (Figures 1 and 2, Table 1). Our main objective was to fill an important geographic gap in proxy records of MIS 11 climate that might aid in paleoclimate modeling of sea level and climate during past warm periods (Kleinen et al., 2014; Otto-Bliesner et al., 2017; Raymo & Mitrovica, 2012). Specifically, we focus on the following questions: Did peak MIS 11 warmth occur in the Arctic Ocean early in the MIS 11 interglacial, as during the Holocene (MIS 1; Kaufman et al., 2009, 2016; Briner et al., 2016) or during the middle or latter part of MIS 11 (Rodrigues et al., 2011)? What were sea ice conditions during MIS 11? Do SST and IRD records suggest abrupt suborbital events punctuating MIS 11 in the way that Heinrich events (HE) punctuated the last glacial period (MIS 4-MIS 2, from 60 to 18 ka; Bassis et al., 2017)? Can paleoceanography of the Arctic, specifically sea ice conditions and the strength of inflowing Atlantic Water, be linked to those in the Nordic seas and North Atlantic Ocean, the northward flowing North Atlantic Current (NAC), and Atlantic Meridional Overturning Circulation (AMOC) (Sévellec et al., 2017)?

2. MIS 11 Terminology

Before proceeding, the following conventions for terminology require clarification. Glacial Termination V (also called Termination 5) was the major deglaciation that occurred during the MIS 12-MIS 11 transition and is used in the traditional sense defined by oxygen isotope records of foraminifera (Broecker & Van Donk, 1970) and other proxies. Some records show suborbital "Younger Dryas-like" reversals during Termination V (Helmke et al., 2005; Kandiano et al., 2012) although there is no formal nomenclature for these. Regarding substage terminology for MIS 11, various authors use different terms and definitions due in part to the subjective nature of defining glacials and interglacials based on choices of alignment of a proxy record to orbital parameters such as precession (e.g., Masson-Delmotte et al., 2006; Ruddiman, 2007). The entire period known as the MIS 11 interglacial is dated from ~424 to 374 ka in the deep-sea benthic foraminiferal $\delta^{18}O$ stack (Lisiecki & Raymo, 2005). Substages of MIS 11 are often referred to using letter (i.e., MIS 11c and 11b; Voelker et al., 2010; Palumbo et al., 2019) or number notation (MIS 11.3 for peak interglacial and subdivisions of 11.22 11.23, and 11.24; Rodrigues et al., 2011). We use the number notation to signify substages or stadial periods when Heinrich-like events occurred during the MIS 11-MIS 10 transition.

The term MIS 11c, used by Kandiano et al. (2007) to designate the interglacial climatic optimum, was later refined to MIS 11c sensu stricto dated from ~420 to 398 ka (Kandiano et al., 2012). In a comparison with the Holocene (MIS 1), Kandiano et al. (2012) also identified an early climatic optimum phase ~420–411 ka and a late phase ~411–398 ka during MIS 11c. Kandiano et al. (2016) also recognized peak interglacial conditions in the Nordic seas during MIS 11c sensu stricto from ~419 to 400 ka when the subpolar planktic foraminifera *Turborotalita quinqueloba* (Natland) co-occurred with the polar species *Neogloboquadrina pachyderma* (Ehrenberg; formerly called *N. pachyderma* sinistral coiling(s); see Darling et al., 2017). In terms of IRD

10.1029/2019PA003708

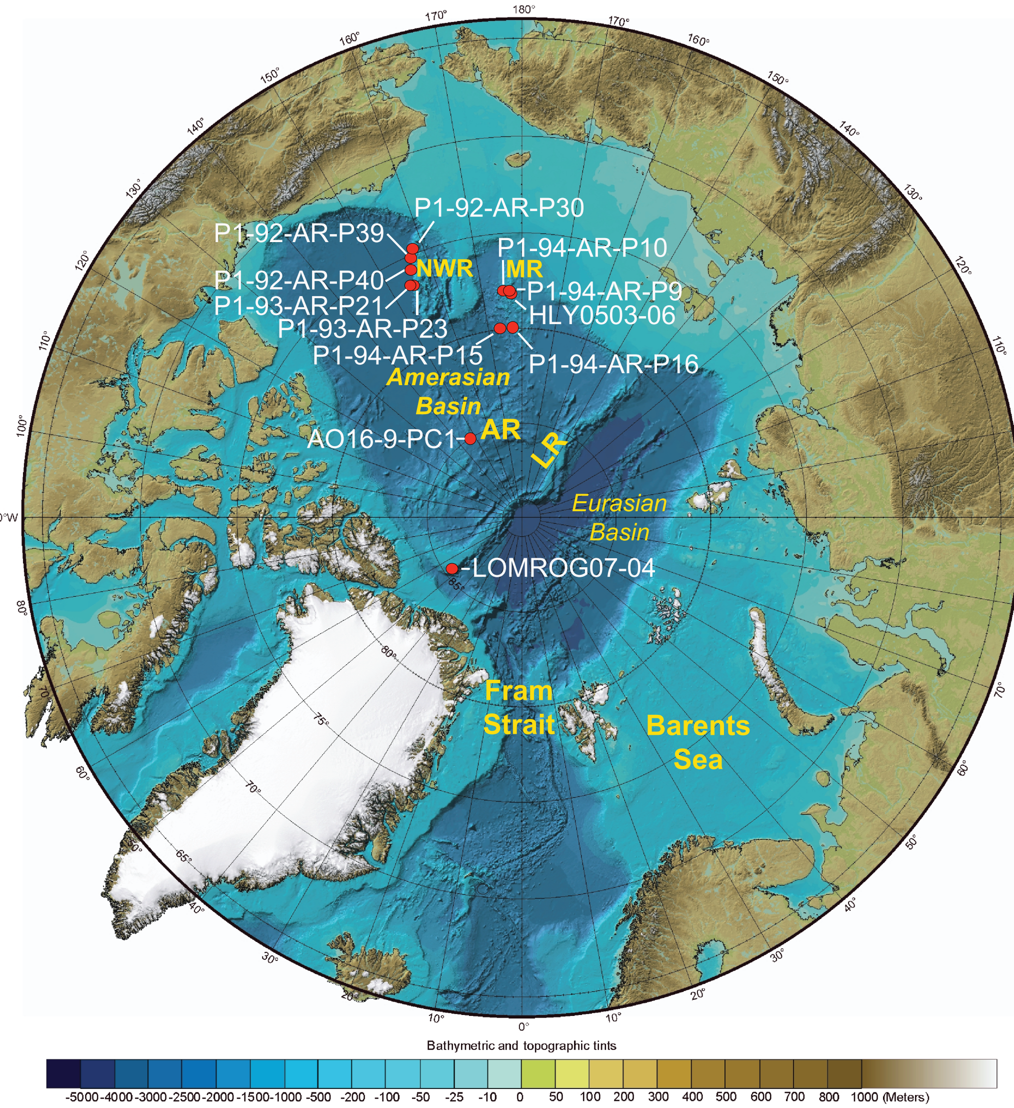

Figure 1. Map showing core locations (red dots) on the Northwind Ridge (NWR), Mendeleev Ridge (MR) and Lomonosov Ridge (LR) for the study of Marine Isotope Stage 11. Basemap from International Bathymetric Chart of the Arctic Ocean Version 3 (Jakobsson et al., 2012).

flux, in the central and eastern Nordic seas, a warm peak comes late as indicated by a phase with no IRD, around 404–406 ka (Kandiano et al., 2016).

In a modeling study of MIS 11 sea level, Raymo and Mitrovica (2012) identified peak eustatic sea level from ~410 to 400 ka, roughly consistent with orbitally tuned marine isotope records and coral reef highstands. As we see below, terminological differences have paleoceanographic implications related to changes in SST, ice rafting, freshwater flux, and other factors. For our study, we consider MIS 11 to be dated at ~424–374 ka, based on the Lisiecki and Raymo (2005) benthic foraminiferal $\delta^{18}O$ stack, and we designate the peak MIS 11 interglacial as MIS 11.3 ~410–400 ka (see below).

Finally, Arctic Quaternary sediments contain a distinct stratigraphic zone dominated by the subpolar planktic foraminiferal taxon referred to as *Turborotalia egelida* (Cifelli & Smith). *T. egelida* may be a morphotype of the species *T. quinqueloba* (Natland), and additional taxonomic and ecological work is needed to refine its usage (O'Regan et al., 2019). Nonetheless, what we call the "*egelida* zone" was recognized in early studies (Backman et al., 2004; Herman, 1974; Poore et al., 1993) and, more recently, shown to be widespread in the Amerasian Basin (Cronin et al., 2014; Polyak et al., 2013) and central Arctic (O'Regan et al., 2019).

10.1029/2019PA003708

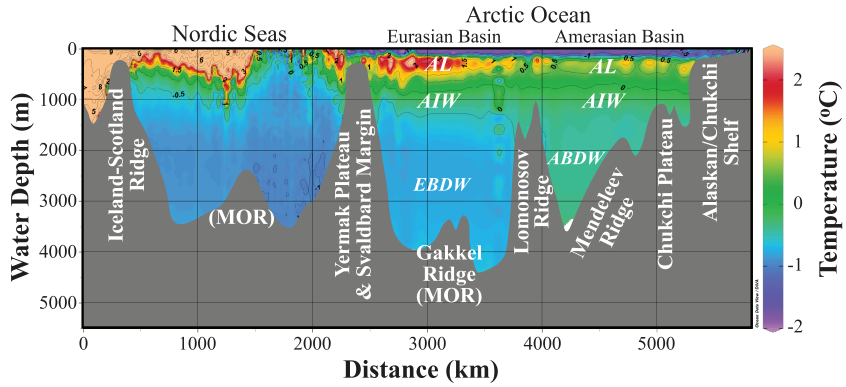

Figure 2. Cross section of key Arctic Ocean locations and Arctic Ocean temperatures from World Ocean Atlas 2013 (https://www.nodc.noaa.gov/OC5/woa13/) plotted using Ocean Data View (ODV, Schlitzer, 2016).

The *egelida* zone is characterized by high abundance of *T. egelida* (up to 90% total assemblage; Cronin et al., 2013), and often relatively small specimens (63–100 μm diameter), in contrast with most interglacial sediments dominated by *Neogloboquadrina pachyderma(s)* (Eynaud et al., 2009).

Typically, the *egelida* zone is between 12 and 63 cm thick depending on the core site sediment accumulation rate (Table 1, see section 5) and contains almost no coarse IRD, minimal sand-sized material, and rare benthic foraminifers. Based on all available chronostratigraphic data for each core, we consider the *egelida* zone to represent the MIS 11 interglacial. In this zone, *T. egelida* specimens can be so abundant that they constitute the dominant element of the lithofacies. Occurrences of the better-known subpolar planktonic foraminifera *T. quinqueloba* are also observed in sediments dated to MIS 11 on the Lomonosov Ridge and also occur intermittently in post-MIS 11 sediments (O'Regan et al., 2019). However, where recognized, the *T. egelida* zone is unique in its high abundance of this distinct enigmatic species/morphotype. Current understanding of Arctic Ocean planktonic foraminifera genetic diversity and biogeography (Darling et al., 2007, 2017) suggests that *T. egelida* represents a subpolar migrant entering the Arctic Ocean from lower latitudes via the NAC either through the eastern Fram Strait or the Barents Sea. Migration from the Pacific Ocean via the Bering Strait cannot be totally excluded. For the current study, we consider the *egelida* zone an extremely useful biomarker for the MIS 11 interglacial in the Arctic Ocean (see Cronin et al., 2013; Marzen et al., 2016).

3. Material and Methods

3.1. Sediment Cores and Ocean Setting

A total of 12 piston cores were studied; 6 yielded new benthic foraminifera stable isotope ($\delta^{18}O_b$) records (Figure 1, Table 1). In addition, two box cores and one trigger core were studied for benthic foraminiferal oxygen isotopes ($\delta^{18}O_b$) over the past ~40 ka. Cores were selected based on the preservation of faunal and geochemical proxies, core stratigraphy and chronology, and their locations in intermediate and deep water masses on the Northwind, Mendeleev, and Lomonosov Ridges (Schlitzer, 2016, Figure 2).

3.2. Chronology

There is a large literature on Quaternary orbital-scale litho-, bio-, and chronostratigraphy in Arctic cores, including studies of planktic foraminifera (Poore et al., 1993), physical properties (color, grain size, and bulk density; O'Regan et al., 2008), oxygen isotopes (Polyak et al., 2004; Spielhagen et al., 2004), manganese layers (Jakobsson et al., 2000; Löwemark et al., 2014), elemental (calcium) concentrations (Wang et al., 2018), and microfossil density (a measure of biological productivity) (Marzen et al., 2016; Wollenburg et al., 2007), among others. Many studies use a cyclostratigraphic approach augmented by biostratigraphy to correlate and date sediments that are too old for radiocarbon dating. Biostratigraphic summaries of Arctic sediments using calcareous nannofossils, planktic and benthic foraminifera, and ostracodes which can be found in Backman et al. (2009), Stein et al. (2010), Polyak et al. (2013), Cronin et al. (2014), and references therein. Additional age data come from amino acid racemization (Kaufman et al., 2008), strontium dating (Dipre

10.1029/2019PA003708

et al., 2018) and Optically Stimulated Luminescence (Jakobsson et al., 2003). Magnetostratigraphy has also been attempted in Arctic sediments (reviewed in Xuan & Channell, 2010), but complications from self-reversals and anomalous excursions preclude its use as a chronological tool (Channell & Xuan, 2009).

Our approach was to use radiocarbon dating of the uppermost 10 to 30 cm of sediment from box and multi-cores (see Poirier et al., 2012), two key foraminiferal markers, *Bolivina aculeata* (a dominant species in MIS 5a, ~80 ka, summarized in Cronin et al., 2014) and the planktic species *Turborotalita egelida* (discussed above, ~400 ka; O'Regan et al., 2019), and cyclostratigraphy of calcareous microfossil density (benthic foraminifera, ostracodes; Marzen et al., 2016). Due to highly varying sedimentation rates during glacial and interglacial cycles, we developed age-depth models for each core using foraminiferal tiepoints and MIS boundaries identified from microfaunal density. These age models are given in Table 2 and illustrated in supporting information Figure S1. The *egelida* zone in the Arctic Ocean, which we recognize in all of the cores discussed here, allowed us to align proxy records from different Arctic cores and correlate with records from the Nordic seas and North Atlantic.

3.3. Calcareous Microfossil Density and Productivity

The Arctic Productivity Index (API) is a composite "stack" constructed using benthic foraminifera and ostracode density data (specimens per gram sediment per kiloannum) from 14 cores, each with its own age model. The API stack was generated by aligning and binning microfossil records to a high-resolution target record and generating an age model for the resulting stacked record by aligning it to the LR04 benthic foraminiferal oxygen isotope ($\delta^{18}O_b$) stack. This method was discussed in detail by Marzen et al. (2016). The group of cores covers 74.6 to 87.1°N latitude and water depths of 700 to 1900 m, thus sampling mainly AIW in the western and central Arctic. Benthic productivity can be measured using ostracode and benthic foraminiferal accumulation rates, which are closely linked to surface ocean productivity and food flux (Marzen et al., 2016; Wollenburg et al., 2004, 2007).

In the Marzen et al. (2016) study, API stacks were created for the first time, one for foraminifera, one for ostracodes, and one for foraminifera and ostracodes combined. Because the aim of the initial study was to examine orbital-scale variability, values were stacked in 2.5 cm bins for a target record with a sedimentation rate of ~0.5–2.5 cm/ka, limiting temporal resolution to events occurring on timescales longer than ~5 kyr. For the current study, we created higher resolution records by using smaller bins (i.e., 0.5, 1, 1.5 and 2 cm) for the stacked curves to examine suborbital patterns.

3.4. Benthic Foraminiferal $\delta^{18}O$

Five species of benthic foraminifera were used for stable isotopic analyses: *Cassidulina teretis*, *Oridosalis tener*, *Cibicidoides wuellerstorfi*, *Pullenia bulloides*, and *Cassidulina reniforme*. Foraminifera were brush-picked, and individual specimens were scored for visual preservation, ranging from 1 (transparent) to 4 (visual signs of alteration, including recrystallization and addition of authigenic mineral coatings). Of the five species, the three most abundant were used to develop the preliminary composite record presented here (*C. teretis*, *O. tener*, and *C. wuellerstorfi*). Discussion of benthic foraminiferal ecology and taxonomy is given in Wollenburg and Mackensen (1998), Osterman et al. (1999), Scott et al. (2008), Seidenstein et al. (2018), and Cronin et al. (2019).

A total of 326 oxygen isotope analyses were obtained, of which 317 analyses were on the 3 most common species; these were used to develop a composite $\delta^{18}O_b$ stack back to 500 ka (see supporting information). A minimum of ~30 μg of foraminiferal calcite (~2–8 individual specimens) was used to perform each stable isotope analysis. Two hundred fifty-six stable isotope analyses were conducted at Rensselaer Polytechnic Institute using an Isoprime dual inlet ratio mass spectrometer. Nineteen $\delta^{18}O_b$ values on *C. wuellerstorfi* from trigger core HLY-0205-18tc were measured on a Thermo Delta V+ with Kiel IV device at the Lamont-Doherty Earth Observatory (LDEO). Additional 46 $\delta^{18}O_b$ values on *C. wuellerstorfi* from box cores AOS94-B16 and AOS94-B17 were previously measured on a Finnigan MAT252 with Kiel device at Woods Hole Oceanographic Institution by Poore et al. (1999) and are included here. All measurements are reported in delta notation relative to Vienna Pee Dee Belemnite (VPDB) corrected to the NBS19 standard, with an average analytical precision (1σ) of $\pm$0.05 (measurements from LDEO and Woods Hole Oceanographic Institution) and (2σ) of $\pm$0.08 (measurements from Rensselaer Polytechnic Institute) on $\delta^{18}O_b$.

10.1029/2019PA003708

Table 1
Core Data for Study of MIS 11 in the Arctic

Core	Core abbreviation	Water Depth (m)	Longitude	Latitude ºN	Geographic Location	*T. egelida* depth (cm)	*T. egelida* Zone Thickness	MIS11-Age/ DepthEq
P1-94-AR-P9	P9	1035	-176.04	78.133	Mendeleev Ridge	413-427	14	y = 5.4054 x - 1862.5
P1-93-AR-P21	P21	1470	-154.21	76.86	Northwind Ridge	202-232	30	y = 2.6592 x - 183.51
P1-92-AR-P30	P30	765	-158.05	75.31	Northwind Ridge	585-625	40	y = 1.1562 x - 287.26
P1-92-AR-P39	P39	1470	-156.03	75.84	Northwind Ridge	288-333	45	y = 0.8365 x + 142.3
P1-92-AR-P40	P40	700	-156.55	76.26	Northwind Ridge	342-405	63	y = 0.7225 x + 118.88
P1-94-AR-P15	P15	2726	-173.32	80.2	Mendeleev Ridge	267-303	36	y = 1.4035x
HLY0503-6	HLY-6	800	-176.29	78.98615	Mendeleev Ridge	175-206	31	Polyak er al 2013
LOMROG04-07	LOMROG-4	811	-53.77	86.7	Lomonosov Ridge	298-310	12	Hanslik et al., 2013
P1-93-AR-P23	P23	951	-155.07	76.95	Northwind Ridge	61-86	25	Polyak er al 2013
P1-94-AR-PC16	PC16	1568	-178.72	80.333	Mendeleev Ridge	209-239	30	y=1.4318 + 80
AO16-9-PC1	16-9PC	2212	-148.33	85.9557	Alpha Ridge	239-250	11	Y=159 x-10.8
P1-94-AR10	P10	1673	-174.633	78.15	Mendeleev Ridge	247-261	14	y = 1.8217 x - 67.318
*HLY0503-18tc	HLY18tc	2654	-146.683	88.45	Lomonosov Ridge	NA	NA	
*Pl-94AR-B17	B17	2217	178.97	81.27	Mendeleev Ridge	NA	NA	
*Pl-94AR-B16	B16	1533	-178.71	80.34	Mendeleev Ridge	NA	NA	

Core	Prior AgeModel**	Sea ice-*Acetabulastoma*	δ18O	Mg/Ca	NADW-*Krithe*	Planktic SSTs	Ostracode Density	Benthic Foram Density
P1-94-AR-P9	2	1	3	4	1		2	2
P1-93-AR-P21	2	3	3	4			2	
P1-92-AR-P30	2	1	3	4	1		2	2
P1-92-AR-P39	2	1	3	4	1		2	2
P1-92-AR-P40	2	1	3	4	1		2	
P1-94-AR-P15	3	3	3					
HLY0503-6	1,6	1		4	1	1	2	2
LOMROG04-07	7	3					2	2
P1-93-AR-P23	1,2,6	1		4				2, 5
P1-94-AR-PC16	1,2	3						
AO16-9-PC1	3	3						
P1-94-AR10	3	3					2	
*HLY0503-18tc			3	x				
*Pl-94AR-B17			3	x				
*Pl-94AR-B16			3	x				

Sources, 1 Cronin et al., 2013, 2014, 2 Marzen et al., 2016, 3 This paper, 4 Cronin et al., 2017, 5 DeNinno et al., 2015, 6 Polyak et al., 2013, Dipre et al., 2018, 7 Hanslik et al., 2013
*Box and trigger cores used for last 40 ka, no orbital-scale sediment **See Supplemental Figure S1 for details of age model for each core.

10.1029/2019PA003708

Table 2
Anchor Points for Orbital-Scale Tuning in the Arctic

						Age Model			
						Segment 1			
Core	Length	*T. egelida* depth		*T. egelida* Thickness	MIS 11 Sedimentation rate	Depth Upper	Depth Lower	Eq#1	Segment 1 Sedimentation Rate
P1-94-AR-P9	748.75	413	427	14	1.0	16	175	y = 0.7342 x + 4.059	1.4
P1-93-AR-P21	303.5	202	232	30	0.5	71	122	y = 0.9055 x + 20.211	1.1
P1-92-AR-P30	764	585	625	40	1.5	2	540	y = 0.6096 x + 7.2797	1.6
P1-92-AR-P39	678	288	333	45	0.8	1	144	y=0.7895 x+5.01	1.3
P1-92-AR-P40	530	367	411	44	1.0	0	166	y = 0.7674* x+3.3866	
P1-94-AR-P15	761	267	303	36	0.7	0	285	y=1.4035x	
HLY0503-6	236	175	206	31	0.5				
LOMROG04-07	514.5	298	310	12	0.8	0.5	117	y = 0.6095 x + 20.894	1.6
P1-93-AR-P23	560.75	61	86	25	0.2	18	168	y = 1.0717 x + 59.616	1.1
P1-94-AR-PC16	650.5	209	239	30	0.6	0	224	y = 1.4318 x + 80	
AO16-9-PC1	749	239	250	11	0.6				
P1-94-AR10	596.5	247	261	14	0.6	0	169	y = 1.0717 x + 59.616	

	Age Model											
	Segment 2				Segment 3				Segment 4			
Core	Depth Upper	Depth Lower	Eq#2	Segment 2 Sedimentation Rate	Depth Upper	Depth Lower	Eq#3	Segment 3 Sedimentation Rate	Depth Upper	Depth Lower	Eq#4	Segment 4 Sedimentation Rate
P1-94-AR-P9	175	309	y = 1.2638 x - 91.453	0.8	309	404	y = 0.3885 x + 179.97		414	423	y = 5.4054 x - 1862.5	
P1-93-AR-P21	122	230	y = 2.6592 x - 183.51	0.4	230	323.5	y = 1.1658 x + 155.87					
P1-92-AR-P30	540	709.5	y = 1.1562 x - 287.26	0.9								
P1-92-AR-P39	144	232.8	y = 2.3169 x - 205.1	0.4	233	336.8	y = 0.8365 x + 142.3					
P1-92-AR-P40	166	200	interpolated		200	250	y = 2.1668 x - 239.98		250	425	y = 0.7225 x + 118.88	
P1-94-AR-P15												
HLY0503-6												
LOMROG04-07	117	304.5	y = 1.6489 x - 102.1	0.6								
P1-93-AR-P23	168	266	y = 1.8217 x - 67.318	0.5								
P1-94-AR-PC16												
AO16-9-PC1												
P1-94-AR10	169	313	y = 1.8217 x - 67.318									

Note. See Supplemental Figure S1 for anchor points and age depth models.

Using published vital effect adjustments (Hoogakker et al., 2010; Kristjánsdóttir et al., 2007), and results from our own data, stable isotope values from *C. teretis* (*C. neoteretis* to some authors; see Cronin et al., 2019) and *O. tener* were adjusted to *C. wuellerstorfi*, which calcifies its test in thermodynamic equilibrium with ambient seawater at low temperatures (Bemis et al., 1998). Adjusted isotope values were used to construct a composite record and scaled to *Uvigerina* by applying a constant adjustment of +0.64‰ (Duplessy et al., 1984; Duplessy et al., 2002; Shackleton & Opdyke, 1973). Due to conflicting vital effect adjustments used in other studies of *C. teretis*, we used paired analyses of *C. wuellerstorfi* and *C. teretis* to evaluate available adjustment values (Poole et al., 1994; Kristjánsdóttir et al., 2007; Groot et al., 2014; Chauhan et al., 2015). Our paired analyses exhibited a +0.45 ± 0.2‰ mean $\delta^{18}O_b$ offset for *C. teretis* from *C. wuellerstorfi*, which is in general agreement with the vital effect adjustment (0.504‰) established by Kristjánsdóttir et al. (2007); see also Lubinski et al., 2001). Therefore, we applied a -0.504‰ adjustment to *C. teretis* stable isotope values, with the caveat that additional work is needed on benthic species $\delta^{18}O_b$ offsets (Bauch et al., 2011; Bauch & Erlenkeuser, 2003).

3.5. Other Proxy Methods

In addition to the API productivity stack and new benthic $\delta^{18}O_b$ records, this paper incorporates proxy records of bottom water temperature (BWT) based on ostracode magnesium/calcium (Mg/Ca) paleothermometry (Cronin et al., 2012, 2017; Farmer et al., 2012), sea ice cover based on abundances of an epipelagic ostracode species (*Acetabulastoma arcticum*; Cronin et al., 2010, 2013), and benthic ostracode taxa that are dominant in modern AIW and AODW (Cronin et al., 2014; Poirier et al., 2012). Results for each proxy record are discussed in section 5.

4. The MIS 11 Interglacial

4.1. Global Records of MIS 11

As background, Figure 3 presents "global" records of the last 800 ka to provide a context for examining the MIS 11 interglacial. Figure 3a is the combined record of atmospheric CO_2 from several Antarctic ice cores showing (1) the ~40 ppmv increase in interglacial CO_2 levels from MIS 13 to MIS 11, during the Mid-Brunhes Event (MBE), roughly 450 to 350 ka, and (2) the sustained high preindustrial-like interglacial CO_2 levels (at or just below 280 ppmv) during MIS 11 from 425 to 398 ka. These MIS 11 CO_2 concentrations, which use the age model of Yin and Berger (2015), remain relatively high for a longer duration compared to shorter periods of preindustrial-like CO_2 during younger interglacials.

Figure 3b shows the Antarctic temperature curve derived from deuterium excess measurements from the EPICA Dome C ice core (Jouzel et al., 2007), which, although not strictly speaking a global temperature proxy, nonetheless exhibit a similar pattern to the CO_2 curve and are considered a general indicator of Southern Hemisphere climate changes. The deuterium record during the MIS 11-MIS 10 transition clearly exhibits large stadial-like fluctuations in temperature during MIS 11.3, 11.2, and 11.1, which are smaller in amplitude but similar to Dansgaard-Oeschger events of the last glacial cycle.

The marine $\delta^{18}O_b$ curve (LR04; Lisiecki & Raymo, 2005; see also Spratt & Lisiecki, 2016), which is a composite "stack" constructed from 57 marine sediment core benthic foraminiferal $\delta^{18}O$ records, is shown in Figure 3c. Oscillations in $\delta^{18}O_b$ in LR04 represent the combined effects of global land ice volume and deep-sea bottom temperature fluctuations over orbital timescales. The curve shows the familiar sawtooth pattern of the "100-kyr" climate cycles of the last 800 ka, a steady decrease in $\delta^{18}O_b$ during the MIS 12-MIS 11 transition (Termination V), and minimal variation during interglacial MIS 11.

The $\delta^{18}O_b$ can be converted to the $\delta^{18}O_{seawater}$ when corrected for BWT changes using Mg/Ca paleothermometry. Elderfield et al. (2012) made such a reconstruction ODP Site 1123 from the Chatham Rise (Figure 3d). Elderfield's $\delta^{18}O_{seawater}$ record represents a global sea level/ice volume curve and, in contrast to the LR04 stack, exhibits large stadial-like variability during the MIS 11-MIS 10 transition. Rohling et al. (2009, 2010) also showed suborbital variability in sea level/ice volume during the MIS 12-MIS 11 transition based on $\delta^{18}O_{seawater}$ constructed from Red Sea planktic foraminiferal $\delta^{18}O$ (see also Rohling et al., 2014). These types of suborbital events are also seen in the Arctic records discussed below.

10.1029/2019PA003708

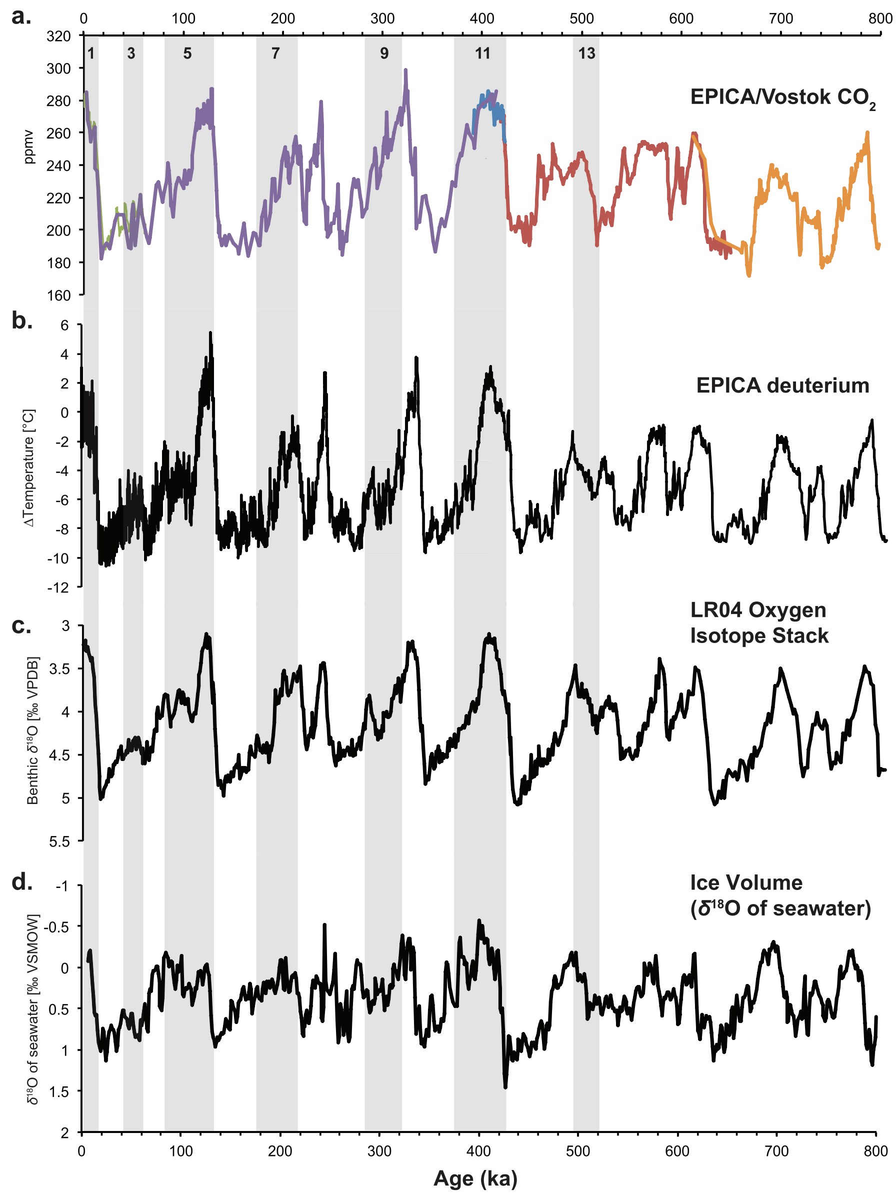

Figure 3. Global paleoclimate records showing pattern during Marine Isotope Stage 11 compared to other interglacial periods. (a) Compilation of Antarctic pCO_2 (atmosphere) records from EPICA Dome C, Taylor Dome, and Vostok ice cores (from Petit et al., 1999; Siegenthaler et al., 2005; Lüthi et al., 2008, and references therein; note that Bereiter et al. (2015) corrected CO_2 measurements from 800 to 600 ka but changes are minor and do not materially affect the CO_2 curve for the MIS 11 interval). (b) Antarctic EPICA deuterium record from Jouzel et al. (2007) plotted as change in temperature. (c) LR04 benthic foraminiferal $\delta^{18}O$ isotope stack compiled from 57 cores (Lisiecki & Raymo, 2005). (d) $\delta^{18}O_{seawater}$ (in ‰ VSMOW) based on benthic foraminiferal $\delta^{18}O_{calcite}$ from ODP site 1123 Chatham Rise from Elderfield et al. (2012).

4.2. Nordic Seas and North Atlantic Marine Records of MIS 12-MIS 10

The warm, saline NAC, which flows into the central Arctic Ocean proper through the eastern Fram Strait and Barents Sea, influences equator-to-pole heat transport and AMOC. The NAC submerges after entering the Arctic forming the subsurface Atlantic Layer (AL), which circulates within the central Arctic Ocean basin. The AL is a critical source of heat bounded above by the Polar Surface Water and below by AIW and Arctic Ocean Deep Water (AODW) (Rudels, 2015). Variability in the temperature and salinity of the NAC and the strength of the AMOC will impact the AL, as well as upper AIW, and is thus critical for correlating suborbital events in the two regions (Bauch, 2013).

Several high-resolution paleoceanographic records from the North Atlantic-Nordic seas region reveal high-amplitude changes in the NAC source water. McManus et al. (1999) first showed at ODP Site 980 in the subpolar North Atlantic Ocean that significant suborbital variability over the last 500 ka occurred when ice sheets reached a critical size. This variability was later confirmed by Helmke and Bauch (2003), Kandiano and Bauch (2007), and Kandiano et al. (2016) for the Nordic seas and in midlatitudes of the northeast North Atlantic by Voelker et al. (2010), Rodrigues et al. (2011), Doherty and Thibodeau (2018), and Kandiano et al. (2017).

Figure 4 shows several of these proxy records for the period MIS 12 through MIS 10 (450 to 350 ka) going from north (top, panel 4a) to south (bottom, panel 4j). These records show that IRD typically increased during Heinrich-like event excursions in both MIS 12-MIS 11 and MIS 11-MIS 10 transitions in the Nordic seas (core MD99-2277) and the North Atlantic (cores M23414, U1313, and core U1308; Hodell et al., 2008). Second, all curves are relatively flat during peak MIS 11 interglacial 410 to 400 ka, reflecting a relatively stable climate with almost no IRD, high SST as derived from alkenones (MD03-2669) and $\delta^{18}O$ of planktic foraminifers (MD99-2277, ODP 980, U1313), and high abundance of *N. pachyderma* (M23414). All benthic $\delta^{18}O$ records (ODP 980, M23414, and U1313), which are probably recording changes in either bottom temperature or strength of overturning circulation, show a similar glacial-to-interglacial pattern with a rapid ~1.8‰ to 2‰ decrease from MIS 12 to MIS 11 and a progressive increase during MIS 11 to MIS 10.

Taken together, these records show that suborbital variability linked to glacial processes and ocean circulation were fundamental features both during Termination V and the MIS 11-10 transition in regions of the Nordic seas and North Atlantic. Transient suborbital cold events during Termination V were likely triggered by freshwater influx from melting ice, perhaps the Greenland Ice Sheet, and they affected surface, middepth, and deeper water layers as well as the AMOC (Kandiano et al., 2017). Similarly, during the transition into the MIS 10 glacial starting about 395 ka, there were multiple cool/warm cycles reflecting a weakening AMOC similar to those seen in HE during the MIS 5a-MIS 3 interval (Voelker et al., 2010).

4.3. Prior Studies of Arctic Ocean Abrupt Climate Events

Several studies have identified glacio-marine sedimentation and ice-rafted events in the Arctic Ocean. For example, Darby et al. (2012) postulated 1,500-year cycles in sea ice drift during the Holocene related to millennial-scale events. Darby et al. (2002) interpreted layers containing iron oxides diagnostic of a North American provenance as times of ice sheet collapse and ice export from the Arctic and linked them to HE known from the North Atlantic Ocean during the last glacial going back to 34 ka. Ice-rafted detrital sediments known as “pink-white” layers (mainly Paleozoic dolomite; Clark et al., 1980; Polyak et al., 2009; Stein et al., 2010) are also widely recognized throughout much of the Arctic for the past ~150 ka and interpreted as evidence for calving events from the Laurentide Ice Sheet. However, there has been no investigation of sediment core records of ice sheet, ice shelf, and sea ice sensitivity during Termination V (MIS 12-MIS 11), within MIS 11, or during the MIS 11-MIS 10 interglacial-to-glacial transition despite their potential importance in high-latitude abrupt climate transitions (McManus et al., 1999).

5. Results

The stratigraphy of Arctic Quaternary sediments provides a necessary context for reconstructing paleoceanographic and glacial history. Marine sediments from Arctic submarine ridges are typically composed of alternating brown (interglacial) and gray/tan (glacial) sediments characterized by changes in density, magnetic susceptibility, manganese content, and calcareous microfossil abundance. Brown interglacial sediments typically have high microfossil density; in glacial intervals, microfossil density is usually lower, although this pattern varies from site to site. Figure 5a shows a photograph of a typical sediment core, the location of detrital pink-white layers, the abundance of microfossils, and key biostratigraphic events including the MIS 11 *egelida* zone. Figures 5b and 5c show three density curves of calcareous microfossil groups (planktic, benthic calcareous foraminifers, and ostracodes), as well as the *egelida* zone, for two other cores. This stratigraphy is recognized throughout most of the Arctic Ocean (Polyak et al., 2009; Poore et al., 1993; Stein et al., 2010 and references therein).

For context for the following discussion, Figure 6 shows the last 600 ka for six proxy records on orbital timescales. Figure 7 shows suborbital variability in expanded curves for the 450–350 ka interval for the API, BWT derived from *Krithe* Mg/Ca, AODW (abundance of the genus *Krithe*) and benthic foraminiferal $\delta^{18}O_b$

10.1029/2019PA003708

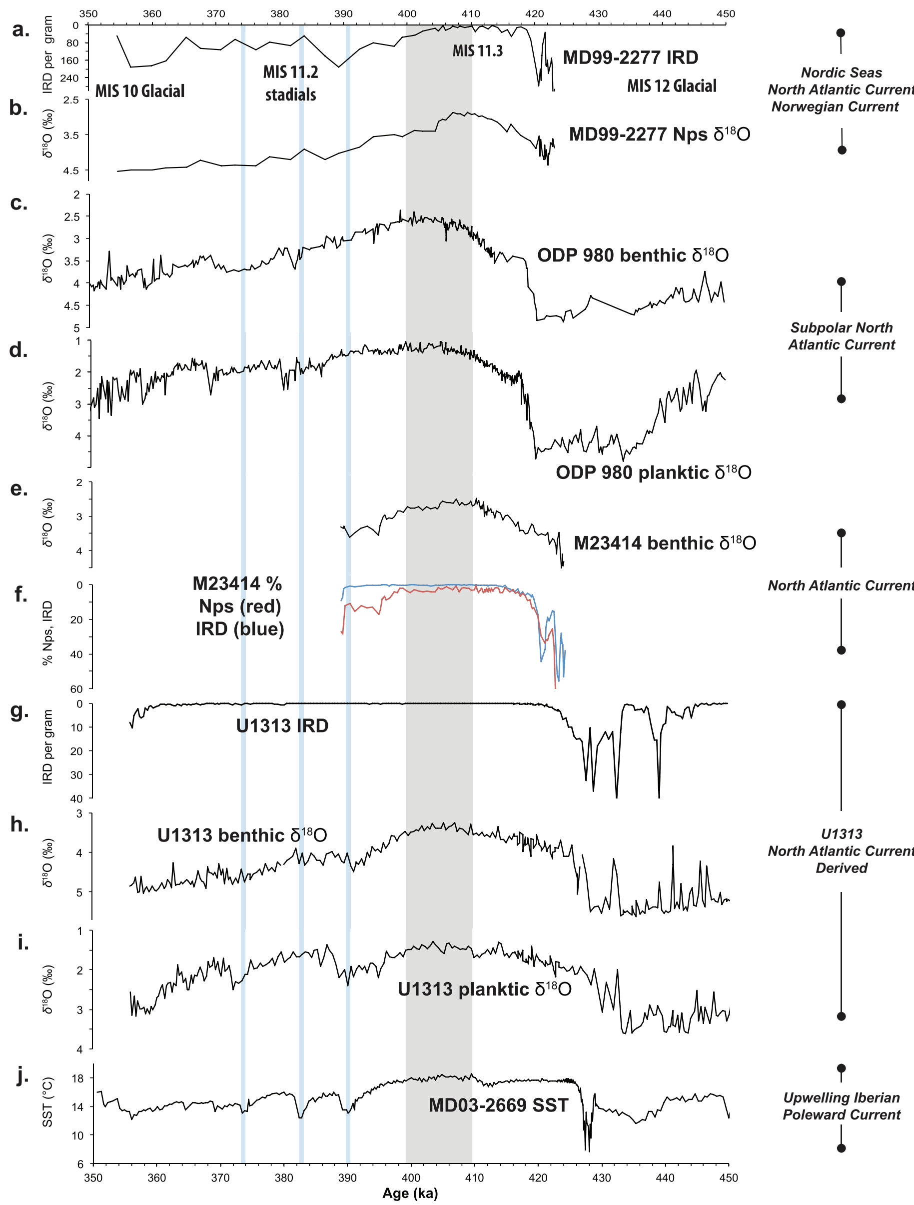

Figure 4. High-resolution paleoceanographic records from the Nordic seas and the northeast Atlantic Ocean (going from north [top] to south [bottom]) showing suborbital variability during Marine Isotope Stages 12-11-10 (450 to 350 ka). (a) Ice-rafted debris (IRD) (grains >250 μm per gram) and (b) $\delta^{18}O$ of *Neogloboquadrina pachyderma* (s) from core MD99-2277 in the Norwegian Sea (Helmke et al., 2005; see also Kandiano et al., 2016); (c) benthic and (d) planktic foraminiferal $\delta^{18}O$ from ODP Site 980 in subpolar North Atlantic (McManus et al., 1999); (e) benthic foraminiferal $\delta^{18}O$ and (f) percent *Neogloboquadrina pachyderma* (s) [red curve] and IRD [blue curve] from core M23414 in northeast Atlantic (North Atlantic Current; Kandiano & Bauch, 2007; Kandiano et al., 2012); (g) IRD, (h) benthic foraminiferal $\delta^{18}O$, and (i) planktic foraminiferal $\delta^{18}O$ from IODP Site U1313 in the North Atlantic Current (Voelker et al., 2010); and (j) sea-surface temperature (SST) from MD03-2669 off Portugal based on alkenones (Rodrigues et al., 2011). Peak interglacial MIS 11.3 and several stadial events are highlighted in vertical shaded regions.

records, as well as the SST reconstructions derived from planktic foraminifers identified by Kandiano in Cronin et al. (2013).

5.1. Arctic Productivity

Arctic productivity tends to be higher and more variable during interglacial periods than during glacial periods (Figure 6a). A notable exception is the period from MIS 9 through MIS 7, where Arctic productivity

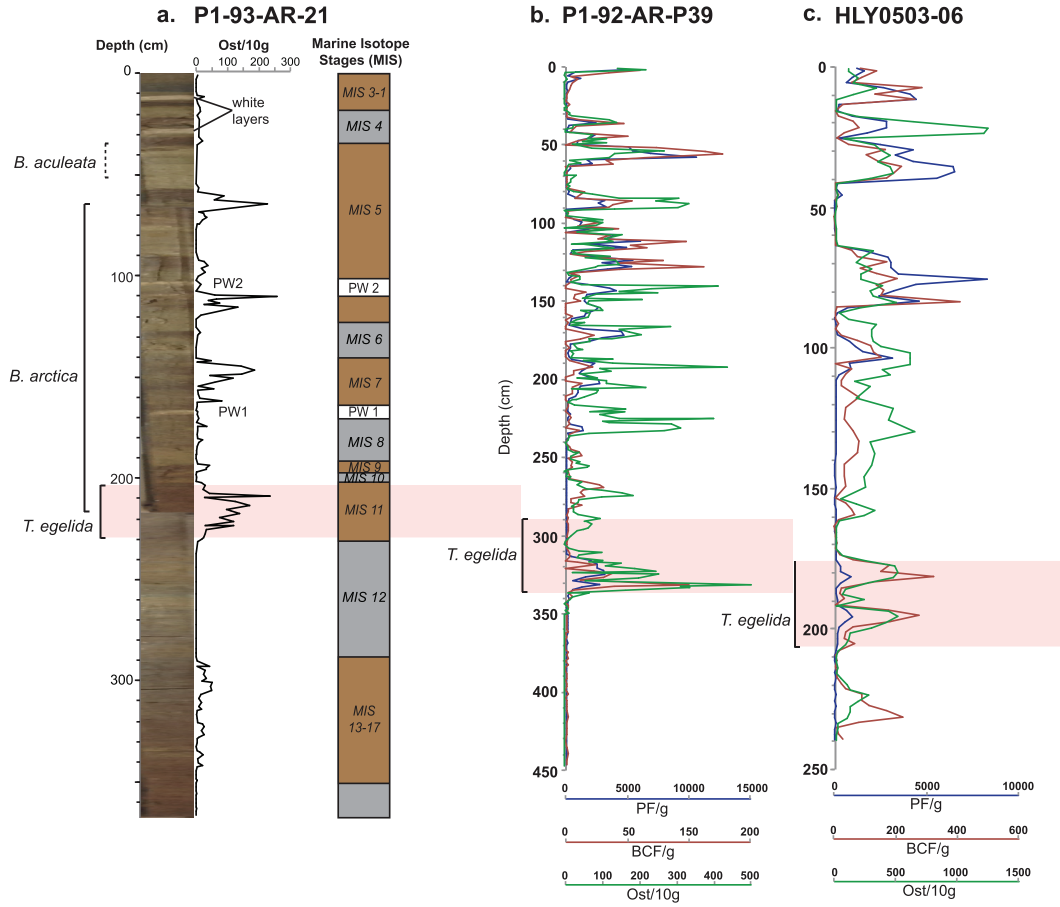

Figure 5. Typical stratigraphy and micropaleontology seen in three Arctic cores showing the location of several key marker beds modified from Cronin et al. (2014). (a) pink-white (PW) layers 1 and 2 of detrital Paleozoic dolomite (Clark et al., 1980), *Bulimina aculeata* (late MIS 5), *Bolivina arctica* (MIS 5-MIS 11), and *Turborotalita egelida* (MIS 11) plotted against Marine Isotope Stages, (b and c) density of planktic foraminifers (PF), benthic foraminifers (BF), and ostracodes (ost) in cores P1-92-AR-P39 and HLY0503-06, respectively.

displays peak values and high variability during MIS 8, a generally weak glacial period. The three productivity peaks during MIS 5 might represent MIS 5.1 (70 ka), MIS 5.3 (100 ka) and MIS 5.5 (125 ka). In the period spanning MIS 12-MIS 10 (Figure 7a), productivity increases steadily with the onset of MIS 11 and subsequently decreases in a gradual manner characterized by high variability during the transition into MIS 10. These patterns are interpreted as signifying suborbital stadial events (see below). Low API values during MIS 10 reflect the presence of thick sea ice and ice shelves limiting the penetration of sunlight and minimal surface productivity.

5.2. BWT

The BWT reconstruction in Figure 6b is derived from the Mg/Ca-temperature calibration of the Arctic ostracode (*Krithe*) (Farmer et al., 2012) applied to several cores covering the last 500 ka (Cronin et al., 2012, 2017). In contrast to deep-sea Mg/Ca records from outside the Arctic, which show deep glacial cooling, the intermediate depth Arctic warms during glacials and stadials due to submerging NAC inflow, forming the AL in the Arctic Ocean, below up to 1 km thick ice shelf cover (Jakobsson et al., 2016; Nilsson et al., 2017). This deep water warming is interpreted to take place due to reduced fresh water influx during colder conditions, in turn causing the cold halocline to deepen and thereby driving the AL deeper (Jakobsson et al., 2016; Nilsson et al., 2017). This can be seen during the last 50 kyr when BWT warming occurs during HE and the Younger Dryas (Cronin et al., 2012, Thornalley et al., 2015).

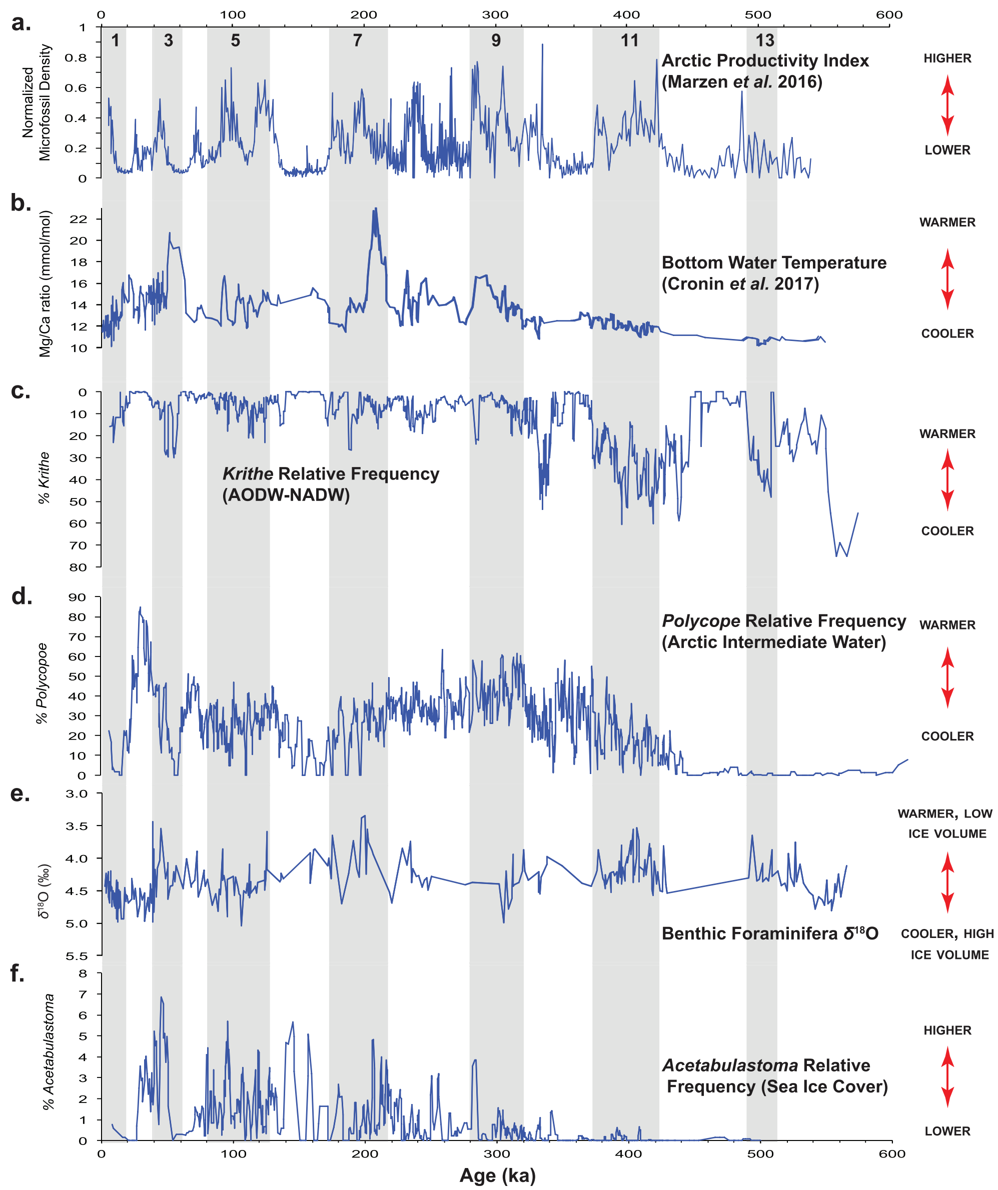

Figure 6. (a) Arctic Productivity Index constructed from benthic foraminiferal and ostracode density curves modified slightly into higher resolution binning from Marzen et al. (2016) using the stacking procedure in Lisiecki and Lisiecki (2002). Arctic productivity is an indicator of biological productivity in benthic ecosystems linked directly to near-surface sea ice cover, algal primary productivity, and surface-to-seafloor food flux. (b) Magnesium/calcium ratios of benthic ostracodes, a measure of BWT (Cronin et al., 2012; Farmer et al., 2012). Curve from Cronin et al. (2017). Note BWT increases during glacial and stadial periods due to the existence of thick ice shelves. (c) Relative frequency (percent abundance) of the genus *Krithe*, an indicator of cold oxygenated Arctic Ocean Deep Water and North Atlantic Deep Water. (d) Relative frequency (percent abundance) of the genus *Polycope*, an indicator of warmer middepth Arctic Intermediate Water; (c and d) modified from Cronin et al. (2014). (e) Benthic foraminiferal $\delta^{18}O_b$ (‰ VPDB on *Uvigerina* scale) uncorrected for BWT or ice volume (see supporting information). (f) Relative frequency (percent abundance) of the species *Acetabulastoma arcticum*, an indicator of perennial sea ice cover.

During MIS 11.3, Arctic Ocean Mg/Ca values were relatively low varying within a ~1 mmol/mol range (Figure 6b). Mg/Ca ratios then gradually increase, punctuated by several cooling events corresponding to MIS 11.2 stadials. There are notable gaps in the composite record during the MIS 12-MIS 10 and MIS 11-MIS 10 transitions, and further studies would be needed to establish this pattern with greater confidence.

In general, however, our records show that MIS 11 bottom temperatures from 700–1500 mwd were similar to temperatures at those depths in the modern Arctic Ocean. Figure 8 shows Mg/Ca ratios converted to °C from

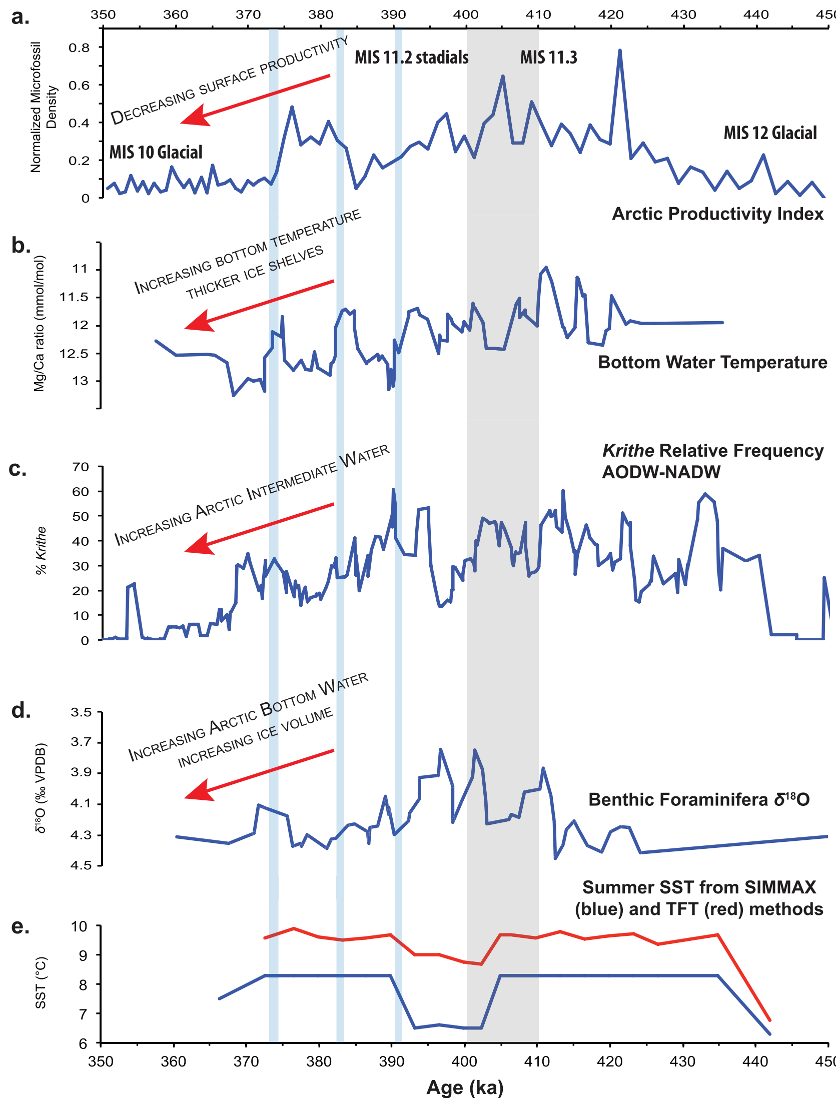

Figure 7. Suborbital paleoceanography for the MIS 12, 11 and 10 interval from 450 to 350 ka, (a) Arctic Productivity Index (API) showing elevated values during peak MIS 11 interglacial conditions. (b) Magnesium/calcium (Mg/Ca) ratios showing low Mg/Ca ratios (lower bottom water temperatures, BWT) during peak MIS 11, and increasing BWT in the MIS 11-MIS 10 transition due to greater AIW influence and the development of thick ice shelves. (c) Relative frequency (RF, percent abundance) of the genus *Krithe*, an indicator of cold oxygenated Arctic Ocean Deep Water and North Atlantic Deep Water, which reaches maximum RFs during several intervals during MIS 11. The decline in % for this genus reflects less AODW, more AIW. (d) Benthic foraminiferal δ^{18}O showing lowest values during peak MIS 11 and increasing values during MIS 11-MIS12 transition due to increasing global ice volume and/or increasing temperature. (e) Estimated sea-surface temperature (SST) based on quantitative planktic foraminiferal assemblage study by E. Kandiano, as described in Cronin et al. (2013). SIMMAX and Transfer Function Technique (TFT) are not ideally suited for Arctic assemblages and estimated temperatures are considered preliminary pending further study.

seven individual cores and compared to modern BWT values at each core site obtained from the World Ocean Atlas. It is clear that at all sites, MIS 11 BWT was roughly similar to modern BWT at the same depth and region of the Arctic Ocean. The most detailed record from core P40 (Northwind Ridge) shows a total range of BWT during peak MIS 11 and the transition into MIS 10 of about 1.5 °C. This range is lower than the BWT range in post-MIS 11 glacial cycles (Figure 6b).

5.3. Arctic Ocean Deep and Intermediate Water

The presence of alternating periods of dominance by AODW and AIW, which may reflect shoaling and deepening of the AIW-AODW boundary, is reflected in the relative abundances of two ostracode genera, *Krithe*

10.1029/2019PA003708

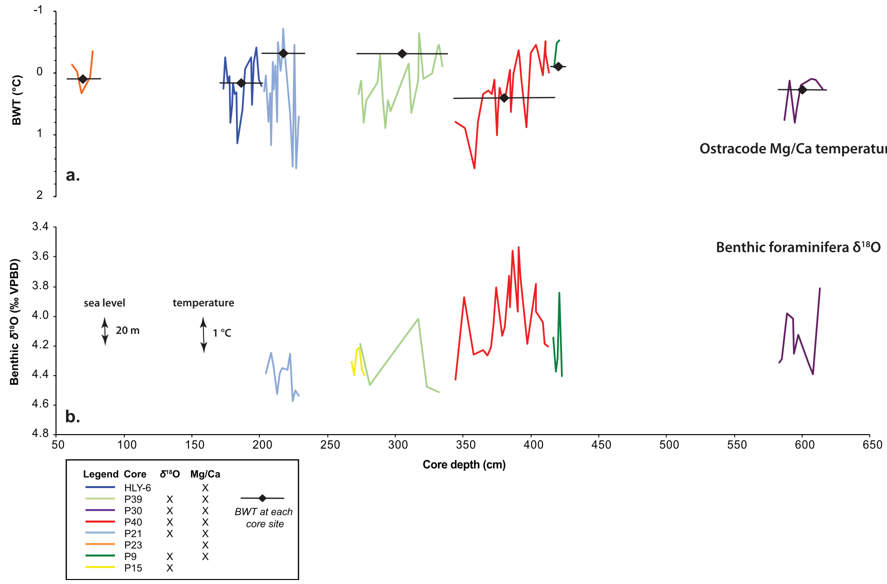

Figure 8. (a) Bottom water temperature estimates based on magnesium/calcium (Mg/Ca) ratios during Marine Isotope Stage 11 from seven Arctic Ocean cores plotted against core depth (cm). Different depths reflect different sedimentation rates. Horizontal bars (diamonds are mean value) give the modern (2005–2012) mean annual BWT from World Ocean Atlas 13 (https://www.nodc.noaa.gov/OC5/woa13/) at each particular core site's water depth from a 1° grid cell near the site. Mg/Ca-temperature calibration 2.279 mmol/mol = 1 °C from Farmer et al. (2012); (b) Oxygen isotope values for benthic foraminifera from MIS 11 in six cores (‰ VPDB). Both seawater temperature and global land ice volume influence $\delta^{18}O$. The scale to the left shows that an increase of 0.25‰ would equal a 1 °C cooling and a 0.1‰ change would equal about 10 m of sea level/ice volume change.

and *Polycope*, respectively. During the MBE, which is centered on MIS 11, *Polycope* frequency increases from near zero at the MIS 12-MIS 11 transition to nearly 60% of the total ostracode assemblage by the onset of MIS 10, reflecting an increase in bottom temperature, probably due to greater AIW influence, during this period (Figure 6d). In contrast, the relative frequency of *Krithe* peaks early during MIS 11, reaching 60% of the total ostracode assemblage, and subsequently declines, nearing zero with the onset of MIS 10 (Figure 6c). Figure 7 shows an expanded view of the decline in *Krithe* abundance throughout the latter part of MIS 11, which indicates a relative decrease in cold AODW, and a relative increase in warmer middepth AIW. The MBE faunal shift from *Krithe*- to *Polycope*-dominated benthic ostracode assemblages is one of the most significant faunal turnovers in the Quaternary history of the Arctic (Cronin et al., 2014) and is similar to that seen in benthic foraminifera from the same regions (Polyak et al., 2013).

5.4. Benthic Foraminiferal $\delta^{18}O$

Figure 6e presents a new benthic foraminiferal $\delta^{18}O$ curve, compiled from nine different cores taken on the Northwind and Mendeleev Ridges (Table 1, supporting information). There are several notable gaps in this record (MIS 6, 8, and 12), due to the problem that calcareous microfossils are often not present in Arctic Ocean cores during glacial intervals, but results nonetheless provide a useful preliminary Arctic benthic $\delta^{18}O$ curve to complement existing global marine $\delta^{18}O$ compilations (LR04 curve; Lisiecki & Raymo, 2005; fig 3).

The $\delta^{18}O$ record is notable in that it does not show the characteristic sawtooth pattern of the LR04 curve shown in Figure 3c. In particular, it lacks the abrupt deglacial decrease, followed by a more gradual increase, in $\delta^{18}O$ values for each 100-kyr glacial cycle. Instead, the record shows gradual changes in $\delta^{18}O$ trends across glacial cycles, as well as evidence for suborbital variability. In addition, the total glacial to interglacial range of $\delta^{18}O$ is about 0.8‰ to 1.0‰, much less than the 1.7‰ to 1.8‰ range in the open ocean. This pattern can likely be explained by the aforementioned influence of warmer BWT (deeper occurrence of AL) during glacial and stadial periods in the Arctic Ocean.

During MIS 11, $\delta^{18}O$ oscillates between higher and lower values between substages 1, 2, and 3, reaching its lowest value (~3.4‰) at MIS 11.3 before the series of stadial events in the latter part of MIS 11 (Figure 7). The entire range of MIS 11 $\delta^{18}O$ values lies between 3.5‰ and 4.5‰; for the most detailed record from P40 the range is 1.0‰ (Figure 8). Figure 8 also shows that for the MIS 11 $\delta^{18}O$ records from six individual cores all display a decrease and subsequent increase in $\delta^{18}O$ values throughout the interglacial. This pattern reflects combined changes in ice volume, temperature, and local hydrographic effects which contribute to the $\delta^{18}O$ signal.

5.5. Paleo-sea Ice

Acetabulastoma arcticum is an epipelagic, sub-sea ice dwelling ostracode species used as an indicator for perennial sea ice. The *Acetabulastoma* record presented in Figure 6 contains data from nine sediment cores taken from the Mendeleev and Northwind Ridges in the western Arctic (HLY6, P10, P21, P23, P30, P39, P40, P9, P16) (Cronin et al., 2014, Figure 9; Cronin et al., 2017, Figure 3, new data from P10, P16). Figure S2a contains a new record from the Alpha Ridge region of the central Arctic (16-9PC). Figure S2b shows a composite record of all sites incorporating the data from this core. Core AO16-9PC fills a notable geographic gap in Arctic paleo-sea ice reconstructions, as few sediment cores have been taken in the region of the Alpha Ridge in the central Arctic due to the presence of thick perennial sea ice. Finally, Figure 8 (upper panel) shows BWT based on ostracode Mg/Ca ratios from the *egelida* zone varied by over 1.0 °C (Cronin et al., 2017) and is approximately the same as modern bottom temperatures (black horizontal lines) near each site obtained from the World Ocean Atlas 13 (https://www.nodc.noaa.gov/OC5/woa13/).

In general, the low abundance of *Acetabulastoma* during MIS 11 is indicative of a seasonally ice-free Arctic, including the Alpha Ridge region in the central Arctic. In addition, the MBE ~450–350 ka was not only a key transition in benthic faunas but also in the occurrence of *Acetabulastoma* and, by inference, extended periods of perennial sea ice that was mostly absent prior to and during MIS 11 (Dipre et al., 2018; Polyak et al., 2013). The pattern of absence of summer sea ice during MIS 11 is in stark contrast to the common perennial sea ice at least during parts of younger interglacials (MIS 1, 3, 5, 7, and 9), which typically have high abundance of *Acetabulastoma*. The absence or low abundance of *Acetabulastoma* during glacial periods is indicative of thick perennial sea ice or ice shelves limiting primary productivity, rather than a seasonally ice-free Arctic.

5.6. SST

Planktic foraminiferal assemblages including common *T. egelida* were used to estimate MIS 11 SST in core HLY6 on the Mendeleev Ridge by E. Kandiano (in Cronin et al., 2013). The two methods included the SIMMAX method of Pflaumann et al. (2003) and a modified transfer function technique. Figure 7e shows estimated elevated summer SST between 440 and 435 ka, beginning at the onset of MIS 11, reaching from 6–7 °C to 8–10 °C during the peak MIS 11 interglacial. SST remained stable throughout the interglacial with the exception of a notable decline in temperature (1–2 °C) between 405 and 390 ka. These results must be considered preliminary as there exists no modern analog data set from surface sediments containing *T. egelida*. Nonetheless, as discussed above, the *T. egelida*-dominated assemblage that is found throughout the Arctic during MIS 11 is in stark contrast to those in younger interglacial periods dominated by *Neogloboquadrina pachyderma*.

5.7. Discussion and Conclusions

Our results lead to a better understanding of MIS 11 in the Arctic on several fronts. Peak MIS 11 warmth in the Arctic Ocean seems to have occurred during the middle of MIS 11 roughly 410 to 400 ka if age models and correlations to extra-Arctic records are correct. SST were as high as 8–10 °C at least for peak interglacial warmth, but additional SST proxy methods are needed. Sea ice conditions during MIS 11 were characterized by seasonally (summer) sea ice-free conditions in many regions. These conclusions support the idea that Arctic Amplification is an inherent feature for at least some Quaternary interglacial periods.

There is also extensive evidence for abrupt suborbital events punctuating the MIS 12-MIS 11-MIS 10 interval. These fluctuations in productivity, BWT, and deep and intermediate water masses (AODW and AIW) most likely represented Heinrich-like events involving extensive ice shelves extending off Laurentide and Fennoscandian Ice Sheets bordering the Arctic. Such events, which punctuated the last glacial period (MIS 4 -MIS 2, 60 to 18 ka) in the Arctic (see above), are also consistent with evidence from submarine geophysical and stratigraphic records of ice shelf grounding on Arctic Ocean submarine ridges (Polyak et al., 2001; Niessen et al., 2013; Jakobsson et al., 2016). The cause of Heinrich-like events along the northern margins of the ice sheets likely involves the influence of warm Atlantic Water flowing under ice shelves at water depths of 500 to >1000 meters as evidenced by Mg/Ca paleothermometry and oxygen isotope records.

Evidence supporting such a mechanism comes from Bassis et al. (2017), who modeled a four-step process for HE over the last 100 kyr. First, ice sheets and associated shelves were in maximum positions during glacial periods, and sills along their margins were depressed by the ice. During the second stage, subsurface ocean warming, in the case of our results shown by Mg/Ca paleotemperatures and $\delta^{18}O$ records, causes melting and ice shelf destabilization. This leads to rapid ice margin retreat and IRD deposition such as that seen in the Arctic during the last two glacial cycles (e.g., Löwemark et al., 2016). Finally, isostatic uplift decreases sill depth and shuts off warm water inflow allowing the ice sheet/shelf margin to readvance. The entire Heinrich cycle lasted less than 1,000 years, which is difficult to definitively identify with low-resolution records in the Arctic. Nonetheless, this hypothesized scenario implies marine-based ice sheet/shelf instability, modeled for Arctic shelves by Nilsson et al. (2017), during the MIS 12-MIS 10 interval forced by sub-ice ocean temperatures, perhaps reflecting AMOC and internal isostatic adjustment mechanisms.

It is not yet possible to draw specific correlations of suborbital events between Arctic cores and those from the Nordic seas and North Atlantic. Nonetheless, the major events in the MIS 11-MIS 10 transition in both regions (Figures 4 and 7) are likely a reflection of the same large-scale events emanating in the Arctic and outflow via the Fram Strait (Myers & Darby, 2015). If confirmed, they support the idea that continued northward flowing NAC water entered the Arctic through Fram Strait during most of the previous glacial cycle (Rasmussen & Thomsen, 2009).

Acknowledgments
This study was funded by the U.S. Geological Survey Land Change Science Program. JRF acknowledges support from the Climate Center at LDEO and NSF DGE-1144155. M. Torresan, U.S. Geological Survey, and Menlo Park helped sample cores (P1-92-AR30, P1-93-AR21, P1-94-AR9, P1-92AR39, P1-92-AR40, and P1-94-AR15), and L. Polyak provided HLY0503-18tc core. We are grateful to H. Dowsett for a helpful review, J. Seidenstein and A. Ruefer for figure editing, and L. Gemery for invaluable graphics help. Supporting data files are available at the U.S. National Climatic Data Center, National Centers for Environmental Information (https://www.ncdc.noaa.gov/data-access/paleoclimatology-data). Any use of trade, firm, or product names is for descriptive purposes only and does not imply endorsement by the U.S. Government.

References

Backman, J., Fornaciari, E., & Rio, D. (2009). Biochronology and paleoceanography of late Pleistocene and Holocene calcareous nannofossil abundances across the Arctic Basin. *Marine Micropaleontology*, *72*(1), 86–98. https://doi.org/10.1016/j.marmicro.2009.04.001

Backman, J., Jakobsson, M., Løvlie, R., Polyak, L., & Febo, L. A. (2004). Is the central Arctic Ocean a sediment starved basin? *Quaternary Science Reviews*, *23*(11), 1435–1454. https://doi.org/10.1016/j.quascirev.2003.12.005

Bassis, J. N., Petersen, S. V., & Mac Cathles, L. (2017). Heinrich events triggered by ocean forcing and modulated by isostatic adjustment. *Nature*, *542*, 332–334. https://doi.org/10.1038/nature21069

Bauch, H. A. (2013). Interglacial climates and the Atlantic meridional overturning circulation: Is there an Arctic controversy? *Quaternary Science Reviews*, *63*, 1–22. https://doi.org/10.1016/j.quascirev.2012.11.023

Bauch, H. A., & Erlenkeuser, H. (2003). Interpreting glacial-interglacial changes in ice volume and climate from subarctic deep water foraminiferal d18O. In A. W. Droxler, R. Z. Poore, & L. H. Burckle (Eds.), *Earth's climate and orbital eccentricity: The Marine Isotope Stage 11 Question* (Vol. 137, pp. 87–102). Washington, DC: American Geophysical Union Monograph Series.

Bauch, H. A., Erlenkeuser, H., Helmke, J. P., & Thiede, J. (2000). A paleoclimatic evaluation of Marine Oxygen Isotope Stage 11 in the high-northern North Atlantic (Nordic seas). *Global and Planetary Change*, *24*(1), 27–39.

Bauch, H. A., Kandiano, E. S., Helmke, J. P., Andersen, N., Rosell-Mele, A., & Erlenkeuser, H. (2011). Climatic bisection of the last interglacial warm period in the polar North Atlantic. *Quaternary Science Reviews*, *30*, 1813–1818.

Bemis, B. E., Spero, H. J., Bijma, J., & Lea, D. W. (1998). Reevaluation of the oxygen isotopic composition of planktonic foraminifera: Experimental results and revised paleotemperature equations. *Paleoceanography*, *13*(2), 150–160. https://doi.org/10.1029/98PA00070

Bereiter, B., Eggleston, S., Schmitt, J., Nehrbass-Ahles, C., Stocker, T. F., Fischer, H., et al. (2015). Revision of the EPICA Dome C CO_2 record from 800 to 600 kyr before present. *Geophysical Research Letters*, *42*, 542–549. https://doi.org/10.1002/2014GL061957

Berger, A., & Loutre, M. F. (2002). An Exceptionally Long Interglacial Ahead? *Science*, *297*(5585), 1287–1288. https://doi.org/10.1126/science.1076120

Bowen, D. Q. (2010). Sea level ~400,000 years ago (MIS 11): Analogue for present and future sea-level? *Climate of the Past*, *6*, 19–29.

Briner, J. P., McKay, N. P., Axford, Y., Bennike, O., Bradley, R. S., de Vernal, A., et al. (2016). Holocene climate change in Arctic Canada and Greenland. *Quaternary Science Reviews*, *147*, 340–364. https://doi.org/10.1016/j.quascirev.2016.02.010

Broecker, W. S., & van Donk, J. (1970). Insolation changes, ice volumes, and the O^{18} record in deep-sea cores. *Reviews of Geophysics*, *8*(1), 169–198. https://doi.org/10.1029/RG008i001p00169

Channell, J. E. T., & Xuan, C. (2009). Self-reversal and apparent magnetic excursions in Arctic sediments. *Earth and Planetary Science Letters*, *284*(1–2), 124–131. https://doi.org/10.1016/j.epsl.2009.04.020

Chauhan, T., Rasmussen, T. L., & Noormets, R. (2015). Paleoceanography of the Barents Sea continental margin, north of Nordaustlandet, Svalbard,during the last 74 ka. *Boreas*, *45*(1), 76-99. DOI:10.1111/bor.12135

Clark, D. L., Whitman, R. R., Morgan, K. A., & Mackey, S. D. (1980). Stratigraphy and glacial-marine sediments of the Amerasian Basin, central Arctic Ocean. *Special Paper Geological Society of America*, *181*, 1–57.

Cronin, T. S., Dwyer, G. K., Caverly, E., Farmer, J., DeNinno, L., Rodriguez-Lazaro, J., & Gemery, L. (2017). Enhanced Arctic Amplification Began at the Mid-Brunhes Event ~400,000 years ago. *Scientific Reports*, *7*. https://doi.org/10.1038/s41598-017-13821-2

Cronin, T. M., DeNinno, L. H., Polyak, L., Caverly, E. K., Poore, R. Z., Brenner, A., et al. (2014). Quaternary ostracode and foraminiferal biostratigraphy and paleoceanography in the western Arctic Ocean. *Marine Micropaleontology*, *111*, 118–133. https://doi.org/10.1016/j.marmicro.2014.05.001

Cronin, T. M., Dwyer, G. S., Farmer, J., Bauch, H. A., Spielhagen, R. F., Jakobsson, M., et al. (2012). Deep Arctic Ocean warming during the last glacial cycle. *Nature Geosci.*, *5*(9), 631–634. https://doi.org/10.1038/ngeo1557

Cronin, T. M., Gemery, L., Briggs, W. M., Jakobsson, M., Polyak, L., & Brouwers, E. M. (2010). Quaternary sea-ice history in the Arctic Ocean based on a new ostracode sea-ice proxy. *Quaternary Science Reviews*, *29*(25), 3415–3429. https://doi.org/10.1016/j.quascirev.2010.05.024

Cronin, T. M., Polyak, L., Reed, D., Kandiano, E. S., Marzen, R. E., & Counsil, E. A. (2013). A 600-ka Arctic sea-ice record from Mendeleev Ridge based on ostracodes. *Quaternary Science Reviews*, *79*, 157–167. https://doi.org/10.1016/j.quascirev.2012.12.010

Cronin, T. M., Seidenstein, J., Keller, K., McDougall, K., Reufer, A., & Gemery, L. (2019). The benthic foraminifera cassidulina from the Arctic Ocean: Application to paleoceanography and biostratigraphy. *Micropaleontology*, *65*(2), 105–125.

Darby, D. A., Bischof, J. F., Spielhagen, R. F., Marshall, S. A., & Herman, S. W. (2002). Arctic ice export events and their potential impact on global climate during the late Pleistocene. *Paleoceanography*, *17*(2), 1025. https://doi.org/10.1029/2001PA000639

Darby, D. A., Ortiz, J. D., Grosch, C. E., & Lund, S. P. (2012). 1,500-year cycle in the Arctic Oscillation identified in Holocene Arctic sea-ice drift. *Nature Geoscience*, *5*(12), 897–900. https://doi.org/10.1038/ngeo1629

Darling, K. F., Kucera, M., & Wade, C. M. (2007). Global molecular phylogeography reveals persistent Arctic circumpolar isolation in a marine planktonic protest. *Proceedings National Academy of Sciences USA*, *104*.

Darling, K. F., Wade, C. M., Siccha, M., Trommer, G., Schulz, H., Abdolalipour, S., & Kurasawa, A. (2017). Genetic diversity and ecology of the planktonic foraminifers Globigerina bulloides, Turborotalita quinqueloba and Neogloboquadrina pachyderma off the Oman margin during the late SW Monsoon. *Marine Micropaleontology*, *137*, 64–77.

de Vernal, A., & Hillaire-Marcel, C. (2008). Natural variability of Greenland climate, vegetation, and ice volume during the past million years. *Science*, *320*(5883), 1622–1625. https://doi.org/10.1126/science.1153929

DeNinno, L. H., Cronin, T. M., Rodriguez-Lazaro, J., & Brenner, A. (2015). An early to mid-Pleistocene deep Arctic Ocean ostracode fauna with North Atlantic affinities. *Palaeogeography, Palaeoclimatology, Palaeoecology*, *419*, 90–99. https://doi.org/10.1016/j.palaeo.2014.07.026

Dipre, G. R., Polyak, L., Kuznetsov, A. B., Oti, E. A., Ortiz, J. D., Brachfeld, S. A., et al. (2018). Plio-Pleistocene sedimentary record from the Northwind Ridge: New insights into paleoclimatic evolution of the western Arctic Ocean for the last 5 Ma. *Arktos*, *4*(1), 1–23. https://doi.org/10.1007/s41063-018-0054-y

Doherty, J. M., & Thibodeau, B. (2018). Cold water in a warm world: Investigating the origin of the Nordic seas' unique surface properties during MIS 11. *Frontiers in Marine Science.*, *5*, 251. https://doi.org/10.3389/fmars.2018.00251

Duplessy, J.-C., Labeyrie, L., & Waelbroeck, C. (2002). Constraints on the ocean oxygen isotopic enrichment between the Last Glacial Maximum and the Holocene: Paleoceanographic implications. *Quaternary Science Reviews*, *21*(1), 315–330. https://doi.org/10.1016/S0277-3791(01)00107-X

Duplessy, J.-C., Shackleton, N. J., Matthews, R. K., Prell, W., Ruddiman, W. F., Caralp, M., & Hendy, C. H. (1984). 13C record of benthic foraminifera in the last interglacial ocean: Implications for the carbon cycle and the global deep water circulation. *Quaternary Research*, *21*(2), 225–243. https://doi.org/10.1016/0033-5894(84)90099-1

Dutton, A., Carlson, A. E., Long, A. J., Milne, G. A., Clark, P. U., DeConto, R., et al. (2015). Sea-level rise due to polar ice-sheet mass loss during past warm periods. *Science*, *349*(6244), aaa4019–aaa4162. https://doi.org/DOI, https://doi.org/10.1126/science.aaa4019

Elderfield, H., Ferretti, P., Greaves, M., Crowhurst, S., McCave, I. N., Hodell, D., & Piotrowski, A. M. (2012). Evolution of ocean temperature and ice volume through the mid-Pleistocene climate transition. *Science*, *337*(6095), 704–709. https://doi.org/10.1126/science.1221294

Eynaud, F., Cronin, T. M., Smith, S. A., Zaragosi, S., Mavel, J., Mary, Y., et al. (2009). Morphological variability of the planktonic foraminifer *Neogloboquadrina pachyderma* from ACEX cores: Implications for late Pleistocene circulation in the Arctic Ocean. *Micropaleontology*, *55*, 101–116.

Farmer, J. R., Cronin, T. M., & Dwyer, G. S. (2012). Ostracode Mg/Ca paleothermometry in the North Atlantic and Arctic oceans: Evaluation of a carbonate ion effect. *Paleoceanography*, *27*, PA2212. https://doi.org/10.1029/2012PA002305

Groot, D. E., Aagaard-Sørensen, S., & Husum, K. (2014). Reconstruction of Atlantic water variability during the Holocene in the western Barents Sea. *Climate of the Past*, *10*(1), 51–62. https://doi.org/10.5194/cp-10-51-2014

Hanslik, D., Löwemark, L., & Jakobsson, M. (2013). Biogenic and detrital-rich intervals in central Arctic Ocean cores identified using x-ray fluorescence scanning. *Polar Research*, *32*(1), 18,386. https://doi.org/10.3402/polar.v32i0.18386

Helmke, J. P., & Bauch, H. A. (2003). Comparison of glacial and interglacial conditions between the polar and subpolar North Atlantic region over the last five climatic cycles. *Paleoceanography*, *18*(2), 1036. https://doi.org/10.1029/2002PA000794

Helmke, J. P., Bauch, H. A., Röhl, U., & Mazaud, A. (2005). Changes in sedimentation patterns of the Nordic seas region across the mid-Pleistocene. *Marine Geology*, *215*(3), 107–122. https://doi.org/10.1016/j.margeo.2004.12.006

Herman, Y. (1974). Arctic Ocean sediments, microfauna, and the climatic record in late Cenozoic time. In Y. Herman (Ed.), *Marine Geology and Oceanography of the Arctic Seas* (pp. 283–348). Berlin Heidelberg: Springer.

Hodell, D. A., Channell, J. E. T., Curtis, J. H., Romero, O. E., & Röhl, U. (2008). Onset of "Hudson Strait" Heinrich events in the eastern North Atlantic at the end of the middle Pleistocene transition (640 ka)? *Paleoceanography*, *23*, PA4218. https://doi.org/10.1029/2008PA001591

Hoogakker, B., Elderfield, H., Oliver, K., & Crowhurst, S. (2010). Benthic foraminiferal oxygen isotope offsets over the last glacial-interglacial cycle. *Paleoceanography*, *25*, PA4229. https://doi.org/10.1029/2009PA001870

Jakobsson, M., Backman, J., Murray, A., & Løvlie, R. (2003). Optically stimulated luminescence dating supports central Arctic Ocean cm-scale sedimentation rates. *Geochemistry, Geophysics, Geosystems*, *4*(2), 1016. https://doi.org/10.1029/2002GC000423

Jakobsson, M., Løvlie, R., Al-Hanbali, H., Arnold, E., Backman, J., & Mörth, M. (2000). Manganese and color cycles in Arctic Ocean sediments constrain Pleistocene chronology. *Geology*, *28*(1), 23–26. https://doi.org/10.1130/0091-7613(2000)28

Jakobsson, M., Mayer, L., Coakley, B., Dowdeswell, J. A., Forbes, S., Fridman, B., et al. (2012). The International Bathymetric Chartof the Arctic Ocean (IBCAO) Version 3.0. *Geophysical Research Letters*, *39*, L12609. https://doi.org/10.1029/2012GL052219

Jakobsson, M., Nilsson, J., Anderson, L., Backman, J., Björk, G., Cronin, T. M., et al. (2016). Evidence for an ice shelf covering the central Arctic Ocean during the penultimate glaciation. *Nature Communications*, *7*(1). https://doi.org/10.1038/ncomms10365

Jouzel, J., Masson-Delmotte, V., Cattani, O., Dreyfus, G., Falourd, S., Hoffmann, G., et al. (2007). Orbital and millennial Antarctic climate variability over the past 800,000 years. *Science*, *317*(5839), 793–796. https://doi.org/10.1126/science.1141038

Kandiano, E., Bauch, H., & Gorodinskiy, A. (2007). Comparison of interglacial climate dynamics in the North Atlantic during the last 420,000 years: Evidence from foraminifera assemblages. Conference or Workshop Item presented at the XVII International Conference on Marine Geology, Moscow. Retrieved from http://oceanrep.geomar.de/6251/

Kandiano, E., & Bauch, H. A. (2007). Phase relationship and surface water mass change in the Northeast Atlantic during Marine Isotope Stage 11 (MIS 11). *Quaternary Research*, *68*(3), 445–455. https://doi.org/doi:10.1016/j.yqres.2007.07.009

Kandiano, E. S., Bauch, H. A., Fahl, K., Helmke, J. P., Röhl, U., Pérez-Folgado, M., & Cacho, I. (2012). The meridional temperature gradient in the eastern North Atlantic during MIS 11 and its link to the ocean–atmosphere system. *Palaeogeography, Palaeoclimatology, Palaeoecology*, *333–334*, 24–39. https://doi.org/10.1016/j.palaeo.2012.03.005

Kandiano, E. S., van der Meer, M. T. J., Bauch, H. A., Helmke, J., Damsté, J. S. S., & Schouten, S. (2016). A cold and fresh ocean surface in the Nordic seas during MIS 11: Significance for the future ocean: Cold and Fresh Nordic Seas During MIS 11. *Geophysical Research Letters*, *43*, 10,929–10,937. https://doi.org/10.1002/2016GL070294

Kandiano, E. S., van der Meer, M. T. J., Schouten, S., Fahl, K., Sinninghe Damsté, J. S., & Bauch, H. A. (2017). Response of the North Atlantic surface and intermediate ocean structure to climate warming of MIS 11. *Scientific Reports*, *7*, 46,192. https://doi.org/10.1038/srep46192

Kaufman, D. S., Axford, Y., Hendeerson, A. C. G., McKay, N. P., Oswald, W. W., Saenger, C., et al. (2016). Holocene climate changes in eastern Beringia (NW North America)—A systematic review of multi-proxy evidence. *Quaternary Science Reviews.*, *147*, 312–339. https://doi.org/10.1016/j.quascirev.2015.10.021

Kaufman, D. S., Polyak, L., Adler, R., Channell, J. E. T., & Xuan, C. (2008). Dating late Quaternary planktonic foraminifer Neogloboquadrina pachyderma from the Arctic Ocean using amino acid racemization. *Paleoceanography*, *23*, PA3224. https://doi.org/10.1029/2008PA001618

Kaufman, D. S., Schneider, D. P., McKay, N. P., Ammann, C. M., Bradley, R. S., Briffa, K. R., et al. (2009). Recent warming reverses long-term Arctic cooling. *Science*, *325*(5945), 1236–1239. https://doi.org/10.1126/science.1173983

Kleinen, T., Hildebrandt, S., Prange, M., Rachmayani, R., Müller, S., Bezrukova, E., et al. (2014). The climate and vegetation of Marine Isotope Stage 11—Model results and proxy-based reconstructions at global and regional scale. *Quaternary International*, *348*, 247–265. https://doi.org/10.1016/j.quaint.2013.12.028

Kopp, R. E., Simons, F. J., Mitrovica, J. X., Maloof, A. C., & Oppenheimer, M. (2009). Probabilistic assessment of sea level during the last interglacial stage. *Nature*, *462*(7275), 863–867. https://doi.org/10.1038/nature08686

Kristjánsdóttir, G. B., Lea, D. W., Jennings, A. E., Pak, D. K., & Belanger, C. (2007). New spatial Mg/Ca-temperature calibrations for three Arctic, benthic foraminifera and reconstruction of north Iceland shelf temperature for the past 4,000 years. *Geochemistry, Geophysics, Geosystems*, *8*, Q03P21. https://doi.org/10.1029/2006GC001425

Lisiecki, L. E., & Lisiecki, P. A. (2002). Application of dynamic programming to the correlation of paleoclimate records. *Paleoceanography*, *17*(4), 1049. https://doi.org/10.1029/2001PA000733

Lisiecki, L. E., & Raymo, M. E. (2005). A Pliocene-Pleistocene stack of 57 globally distributed benthic δ18O records. *Paleoceanography*, *20*, PA1003. https://doi.org/10.1029/2004PA001071

Löwemark, L., Chao, W.-S., Gyllencreutz, R., Hanebuth, T. J. J., Chiu, P.-Y., Yang, T.-N., et al. (2016), Variations in glacial and interglacial marine conditions over the last two glacial cycles off northern Greenland. *Quaternary ScienceReviews*, *147*, 164-177. https://doi.org/10.1016/j.quascirev.2015.10.035

Löwemark, L., März, C., O'Regan, M., & Gyllencreutz, R. (2014). Arctic Ocean Mn-stratigraphy: genesis, synthesis and inter-basin correlation. *Quaternary Science Reviews*, *92*, 97–111. https://doi.org/10.1016/j.quascirev.2013.11.018

Lubinski, D. J., Polyak, L., & Forman, S. L. (2001). Freshwater and Atlantic water inflows to the deep northern Barents and Kara seas since ca 13 ^{14}C ka: foraminifera and stable isotopes. *Quaternary Science Reviews*, *20*(18), 1851–1879. https://doi.org/10.1016/S0277-3791(01)00016-6

Lüthi, D., le Floch, M., Bereiter, B., Blunier, T., Barnola, J. M., Siegenthaler, U., et al. (2008). High-resolution carbon dioxide concentration record 650,000–800,000 years before present. *Nature*, *453*(7193), 379–382. https://doi.org/10.1038/nature06949

Marzen, R. E., DeNinno, L. H., & Cronin, T. M. (2016). Calcareous microfossil-based orbital cyclostratigraphy in the Arctic Ocean. *Quaternary Science Reviews*, *149*, 109–121. https://doi.org/10.1016/j.quascirev.2016.07.004

Masson-Delmotte, V., Dreyfus, G., Braconnot, P., Johnsen, S., Jouzel, J., Kageyama, M., et al. (2006). Past temperature reconstructions from deep ice cores: relevance for future climate change. *Climate of the Past*, *2*, 399–448.

McManus, J. F., Oppo, D. W., & Cullen, J. L. (1999). A 0.5-million-year record of millennial-scale climate variability in the North Atlantic. *Science*, *283*(5404), 971. https://doi.org/10.1126/science.283.5404.971

Milker, Y., Rachmayani, R., Weinkauf, M., Prange, M., Raitzsch, M., Schulz, M., & Kucera, M. (2013). Global and regional sea surface temperature trends during Marine Isotope Stage 11. *Climate of the Past*, *9*(5), 2231–2252.

Myers, W., & Darby, D. (2015). A new age model for the central Arctic reveals brief intervals of extreme sedimentation rates over the last 140 kyr. *Arktos*, *1*(1), 1–20. https://doi.org/10.1007/s41063-015-0009-5

Niessen, F., Hong, J. K., Hegewald, A., Matthiessen, J., Stein, R., Kim, H., et al.(2013). Repeated Pleistocene glaciation of the East Siberian continental margin. *Nature Geoscience*, *6*, 842-846. DOI:10.1038/NGEO1904

Nilsson, J., Jakobsson, M., Borstad, C., Kirchner, N., Björk, G., Pierrehumbert, R. T., & Stranne, C. (2017). Ice-shelf damming in the glacial Arctic Ocean: dynamical regimes of a basin-covering kilometre thick ice shelf. *The Cryosphere*, *11*(4), 1745–1765. https://doi.org/10.5194/tc-2017-37

Olson, S. L., & Hearty, P. J. (2009). A sustained +21-m sea-level highstand during MIS 11 (400 ka): direct fossil and sedimentary evidence from Bermuda. *Quaternary Science Reviews*, *28*(3), 271–285. https://doi.org/10.1016/j.quascirev.2008.11.001

O'Regan, M., Coxall, H. K., Cronin, T. M., Gyllencreutz, R., Jakobsson, M., Kaboth, S., et al. (2019). Stratigraphic occurrences of sub-polar Planktic foraminifera in Pleistocene Sediments on the Lomonosov Ridge, Arctic Ocean. *Frontiers in Earth Science*, *7*. https://doi.org/10.3389/feart.2019.00071

O'Regan, M., King, J., Backman, J., Jakobsson, M., Pälike, H., Moran, K., et al. (2008). Constraints on the Pleistocene chronology of sediments from the Lomonosov Ridge. *Paleoceanography*, *23*, PA1S19. https://doi.org/10.1029/2007PA001551

Osterman, L. E., Poore, R. Z., & Foley, K. M. (1999). Distribution of benthic foraminifers (125 Um) in the surface sediments of the Arctic Ocean. USGS Bulletin 2164, 28 pp., U.S. Government Printing Office.

Otto-Bliesner, B. L., Jahn, A., Feng, R., Brady, E. C., Hu, A., & Löfverström, M. (2017). Amplified North Atlantic warming in the late Pliocene by changes in Arctic gateways: Arctic gateways and Pliocene climate. *Geophysical Research Letters*, *44*, 957–964. https://doi.org/10.1002/2016GL071805

Palumbo, E., Voelker, A. H. L., Flores, J. A., & Amore, O. F. (2019). Surface-ocean dynamics during eccentricity minima: A comparison between interglacial Marine Isotope Stage (MIS) 1 and MIS 11 on the Iberian Margin. *Global and Planetary Change*, *172*, 242–255. https://doi.org/10.1016/j.gloplacha.2018.10.011

Past Interglacials Working Group of PAGES (2016). Interglacials of the last 800,000 years. *Reviews of Geophysics*, *54*, 162–219. https://doi.org/10.1002/2015RG000482

Petit, J. R., Jouzel, J., Raynaud, D., Barkov, N. I., Barnola, J.-M., Basile, I., et al. (1999). Climate and atmospheric history of the past 420,000 years from the Vostok ice core, Antarctica. *Nature*, *399*(6735), 429–436. https://doi.org/10.1038/20859

Pflaumann, U., Sarnthein, M., Chapman, M. R., d'Abreu, L., Funnell, B., Huels, M., et al. (2003). Glacial North Atlantic: Sea-surface conditions reconstructed by GLAMAP 2000. *Paleoceanography*, *18*(3), 1065. https://doi.org/10.1029/2002PA000774

Poirier, R. K., Cronin, T. M., Briggs, W. M., & Lockwood, R. (2012). Central Arctic paleoceanography for the last 50 kyr based on ostracode faunal assemblages. *Marine Micropaleontology*, *88–89*, 65–76. https://doi.org/10.1016/j.marmicro.2012.03.004

Polyak, L., Best, K. M., Crawford, K. A., Council, E. A., & St-Onge, G. (2013). Quaternary history of sea ice in the western Arctic Ocean based on foraminifera. *Quaternary Science Reviews*, *79*, 145–156. https://doi.org/10.1016/j.quascirev.2012.12.018

Polyak, L., Bischof, J., Ortiz, J. D., Darby, D. A., Channell, J. E. T., Xuan, C., et al. (2009). Late Quaternary stratigraphy and sedimentation patterns in the western Arctic Ocean. *Global and Planetary Change*, *68*(1–2), 5–17. https://doi.org/10.1016/j.gloplacha.2009.03.014

Polyak, L., Curry, W. B., Darby, D. A., Bischof, J., & Cronin, T. M. (2004). Contrasting glacial/interglacial regimes in the western Arctic Ocean as exemplified by a sedimentary record from the Mendeleev Ridge. *Palaeogeography, Palaeoclimatology, Palaeoecology*, *203*(1), 73–93. https://doi.org/10.1016/S0031-0182(03)00661-8

Polyak, L., Edwards, M. H., Coakley, B. J., & Jakobsson, M. (2001). Ice shelves in the Pleistocene Arctic Ocean inferred from glaciogenic deep-sea bedforms. *Nature*, *410*, 453–457.

Poole, D., Skitem, J., & Vorren, T. O. (1994). Foraminiferal stratigraphy, palaeoenvironments and sedimentation of the glacigenic sequence southwest of Bjørrnøya. *Boreas*, *23*(2), 122–138. https://doi.org/10.1111/j.1502-3885.1994.tb00593.x

Poore, R. Z., Osterman, L., Curry, W. B., & Phillipa, R. L. (1999). Late Pleistocene and Holocene meltwater events in the western Arctic Ocean. *Geology*, *27*(8), 759–762.

Poore, R. Z., Phillips, R. L., & Rieck, H. J. (1993). Paleoclimate record for Northwind Ridge, western Arctic Ocean. *Paleoceanography*, *8*(2), 149–159.

Rasmussen, T. L., & Thomsen, E. (2009). Ventilation changes in intermediate water on millennial time scales in the SE Nordic seas, 65-14 kyr BP. *Geophysical Research Letters*, *36*, L01601. https://doi.org/10.1029/2008GL036563

Raymo, M. E., & Mitrovica, J. X. (2012). Collapse of polar ice sheets during the stage 11 interglacial. *Nature*, *483*(7390), 453–456. https://doi.org/10.1038/nature10891

Rodrigues, T., Voelker, A. H. L., Grimalt, J. O., Abrantes, F., & Naughton, F. (2011). Iberian Margin sea surface temperature during MIS 15 to 9 (580–300 ka): Glacial suborbital variability versus interglacial stability. *Paleoceanography*, *26*, PA1204. https://doi.org/10.1029/2010PA001927

Rohling, E. J., Braun, K., Grant, K., Kucera, M., Roberts, A. P., Siddall, M., & Trommer, G. (2010). Comparison between Holocene and Marine Isotope Stage-11 sea-level histories. *Earth and Planetary Science Letters*, *291*(1), 97–105. https://doi.org/10.1016/j.epsl.2009.12.054

Rohling, E. J., Foster, G. L., Grant, K. M., Marino, G., Roberts, A. P., Tamisiea, M. E., & Williams, F. (2014). Sea-level and deep-sea-temperature variability over the past 5.3 million years. *Nature*, *508*(7497), 477–482. https://doi.org/10.1038/nature13230

Rohling, E. J., Grant, K., Bolshaw, M., Roberts, A. P., Siddall, M., Hemleben, C., & Kucera, M. (2009). Antarctic temperature and global sea level closely coupled over the past five glacial cycles. *Nature Geoscience*, *2*(7), 500–504. https://doi.org/10.1038/ngeo557

Ruddiman, W. F. (2007). The early anthropogenic hypothesis: Challenges and responses. *Reviews of Geophysics*, *45*, RG4001. https://doi.org/10.1029/2006RG000207

Rudels, B. (2015). Arctic Ocean circulation, processes and water masses: A description of observations and ideas with focus on the period prior to the International Polar Year 2007-2009. *Progress in Oceanography*, *132*, 22-67. https://doi.org/10.1016/j.pocean.2013.11.006

Schlitzer, R., 2016, Ocean Data View, odv.awi.de.

Scott, D. B., Schell, T., Rochon, A., & Blasco, S. (2008). Benthic foraminifera in the surface sediments of the Beaufort Shelf and slope, Beaufort Sea, Canada: Applications and implications for past sea-ice conditions. *Journal of Marine Systems*, *74*(3), 840–863. https://doi.org/10.1016/j.jmarsys.2008.01.008

Seidenstein, J. L., Cronin, T. M., Gemery, L., Keigwin, L. D., Pearce, C., Jakobsson, M., et al. (2018). Late Holocene paleoceanography in the Chukchi and Beaufort Seas, Arctic Ocean, based on benthic foraminifera and ostracodes. *Arktos*, *4*(1), 1–17. https://doi.org/10.1007/s41063-018-0058-7

Sévellec, F., Federov, A. V., & Liu, W. (2017). Arctic sea-ice decline weakens the Atlantic Meridional Overturning Circulation. *Nature Climate Change*, *7*, 604-612. DOI:10.1038/NCLIMATE3353

Shackleton, N. J., & Opdyke, N. D. (1973). Oxygen isotope and palaeomagnetic stratigraphy of equatorial Pacific core V28-238: Oxygen isotope temperatures and ice volumes on a 105 and 106 year scale. *Quaternary Research*, *3*(1), 39–55. https://doi.org/10.1016/0033-5894(73)90052-5

Siegenthaler, U., Stocker, T. F., Monnin, E., Lüthi, D., Schwander, J., Stauffer, B., et al. (2005). Stable carbon cycle-climate relationship during the late Pleistocene. *Science*, *310*(5752), 1313–1317. https://doi.org/10.1126/science.1120130

Spielhagen, R. F., Baumann, K.-H., Erlenkeuser, H., Nowaczyk, N. R., Nørgaard-Pedersen, N., Vogt, C., & Weiel, D. (2004). Arctic Ocean deep-sea record of northern Eurasian ice sheet history. *Quaternary Science Reviews*, *23*(11), 1455–1483. https://doi.org/10.1016/j.quascirev.2003.12.015

Spratt, R. M., & Lisiecki, L. E. (2016). A Late Pleistocene sea level stack. *Climate of the Past*, *12*(4), 1079–1092. https://doi.org/10.5194/cp-12-1079-2016

Stein, R., Matthiessen, J., Niessen, F., Krylov, A., Nam, S., & Bazshenova, E. (2010). Towards a better (litho-) stratigraphy and reconstruction of Quaternary paleoenvironment in the Amerasian Basin (Arctic Ocean). *Polarforschung*, *79*, 97–121.

Thibodeau, B., Bauch, H. A., & Knies, J. (2018). Impact of Arctic shelf summer stratification on Holocene climate variability. *Quaternary Science Reviews*, *191*, 229–237. https://doi.org/10.1016/j.quascirev.2018.05.017

Thornalley, D. J. R., Bauch, H. A., Gebbie, G., Guo, W., Ziegler, M.,Bernasconi, S. M., et al. (2015). A warm and poorly ventilated deep Arctic Mediterranean during the last glacial period. *Science*, *349*(#6249), 706-710. DOI:10.1126/science.aaa9554

Voelker, A. H. L., Rodrigues, T., Billups, K., Oppo, D. W., McManus, J. F., Stein, R., ... Grimalt, J. O. (2010). Variations in mid-latitude North Atlantic surface water properties during the mid-Brunhes (MIS 9–14) and their implications for the thermohaline circulation. *6*(4), 531–552. https://doi.org/10.7916/D8639PHB

10.1029/2019PA003708

Wang, R., Polyak, L., Xiao, W., Wu, L., Zhang, T., & Sun, Y. (2018). Late-Middle Quaternary lithostratigraphy and sedimentation patterns on the Alpha Ridge, central Arctic Ocean: Implications for Arctic climate variability on orbital time scales. *Quaternary Science Reviews*, *181*, 93–108. https://doi.org/10.1016/j.quascirev.2017.12.006

Willeit, M., Ganopolski, A., Calov, R., & Brovkin, V. (2019). Mid-Pleistocene transition in glacial cycles explained by declining CO_2 and regolith removal. *Science Advances*, *5*(4), eaav7337. https://doi.org/10.1126/sciadv.aav7337

Wollenburg, J. E., Knies, J., & Mackensen, A. (2004). High-resolution paleoproductivity fluctuations during the past 24 kyr as indicated by benthic foraminifera in the marginal Arctic Ocean. *Palaeogeography, Palaeoclimatology, Palaeoecology*, *204*(3), 209–238. https://doi.org/10.1016/S0031-0182(03)00726-0

Wollenburg, J. E., & Mackensen, A. (1998). Living benthic foraminifers from the central Arctic Ocean: faunal composition, standing stock and diversity. *Marine Micropaleontology*, *34*, 153–185.

Wollenburg, J. E., Mackensen, A., & Kuhnt, W. (2007). Benthic foraminiferal biodiversity response to a changing Arctic palaeoclimate in the last 24,000 years. *Palaeogeography, Palaeoclimatology, Palaeoecology*, *255*(3), 195–222. https://doi.org/10.1016/j.palaeo.2007.05.007

Xuan, C., & Channell, J. E. T. (2010). Origin of apparent magnetic excursions in deep-sea sediments from Mendeleev-Alpha Ridge, Arctic Ocean. *Geochemistry, Geophysics, Geosystems*, *11*, Q02003. https://doi.org/10.1029/2009GC002879

Yin, Q., & Berger, A. (2015). Interglacial analogues of the Holocene and its natural near future. *Quaternary Science Reviews*, *120*, 28–46. https://doi.org/10.1016/j.quascirev.2015.04.008